Journal of Cosmology and Astroparticle Physics
An IOP and SISSA journal

Received: June 23, 2025
Revised: August 20, 2025
Accepted: September 10, 2025
Published: October 16, 2025

Testing quantum-corrected black holes with QPOs observations: a study of particle dynamics and accretion flow

G. Mustafa[a], **Sushant G. Ghosh**[b,c], **Orhan Donmez**[d], **S.K. Maurya**[e,f], **Shakhzod Orzuev**[g,h] **and Farruh Atamurotov**[i,j,k]

[a] *Department of Physics, Zhejiang Normal University, Jinhua 321004, People's Republic of China*
[b] *Centre for Theoretical Physics, Jamia Millia Islamia, New Delhi 110025, India*
[c] *Astrophysics and Cosmology Research Unit, School of Mathematics, Statistics and Computer Science, University of KwaZulu-Natal, Private Bag 54001, Durban 4000, South Africa*
[d] *College of Engineering and Technology, American University of the Middle East, Egaila 54200, Kuwait*
[e] *Department of Mathematical and Physical Sciences, College of Arts and Sciences, University of Nizwa, Nizwa 616, Oman*
[f] *Research Center of Astrophysics and Cosmology, Khazar University, Baku, AZ1096, 41 Mehseti Street, Azerbaijan*
[g] *New Uzbekistan University, Movarounnahr Str. 1, Tashkent 100000, Uzbekistan*
[h] *Institute of Fundamental and Applied Research, National Research University TIIAME, Kori Niyoziy 39, Tashkent 100000, Uzbekistan*
[i] *Kimyo International University in Tashkent, Shota Rustaveli str. 156, Tashkent 100121, Uzbekistan*
[j] *University of Tashkent for Applied Sciences, Str. Gavhar 1, Tashkent 100149, Uzbekistan*
[k] *Tashkent State Technical University, Tashkent 100095, Uzbekistan*

E-mail: gmustafa3828@gmail.com, sghosh2@jmi.ac.in, orhan.donmez@aum.edu.kw, sunil@unizwa.edu.om, shakhzodorzuev@gmail.com, atamurotov@yahoo.com

Abstract: We study the epicyclic oscillations of test particles around rotating quantum-corrected black holes (QCBHs), characterized by mass M, spin a, and the quantum deformation parameter b. By deriving the radial (Ω_r) and vertical (Ω_θ) oscillation frequencies,

https://doi.org/10.1088/1475-7516/2025/10/068

JCAP10(2025)068

we explore their dependence on spacetime parameters and show that quantum corrections ($b \neq 0$) significantly modify the dynamics compared to the classical Kerr case. Through numerical modeling of accretion around QCBHs, we further examine how b influences strong-field phenomena, comparing the results with test-particle dynamics and observational data. Our analysis reveals: (1) Quantum corrections shift the ISCOs outward, with b altering the effective potential and conditions for stable circular motion. (2) The curvature of the potential and thus the epicyclic frequencies change Ω_r shows up to 25% deviation for typical b values, underscoring sensitivity to quantum effects. (3) Precession behavior is modified: while Lense-Thirring precession (Ω_{LT}) remains primarily governed by a, periastron precession (Ω_P) is notably affected by b, especially near the black hole. (4) Accretion disk simulations confirm the physical effects of b, which is aligned well with the test particle analysis. In addition, the quasiperiodic oscillation (QPO) frequencies obtained via both approaches agree with the observed low-frequency QPOs from sources like GRS $1915+105$, GRO $J1655{-}40$, XTE $J1550{-}564$, and $H1743{-}322$. The distinct frequency profiles and altered ratios offer observational signatures that may distinguish QCBHs from classical black holes. Our findings present testable predictions for X-ray timing and a new avenue to constrain quantum gravity parameters.

Keywords: Exact solutions, black holes and black hole thermodynamics in GR and beyond, gravity, quantum black holes

ArXiv ePrint: 2506.16405

JCAP10(2025)068

Contents

1 Introduction

Einstein's general relativity (GR) remains a cornerstone of modern physics, providing the foundational framework for spacetime and gravitation [1]. Its predictions, from Mercury's perihelion precession to gravitational lensing, have been rigorously confirmed [2, 3]. By the mid 20th century, GR became essential in modeling compact objects (e.g., black holes [4]) and cosmology (e.g., cosmic expansion [5]). Despite its success, GR faces challenges in extreme regimes, motivating ongoing tests [2]. Since then, it has become essential to explain astrophysical events related to compact objects and understand the overall structure of the universe [6–11].

Lately, there has been significant progress in understanding the impacts of quantum corrections on rotating black holes (BHs) [12, 13]. Different studies have proposed and examined quantum corrected (QC) versions of the Kerr BH [14], a classical solution for rotating BHs [15]. The results indicate that quantum corrections influence the properties of observable BH [16], providing new illustrations of QCBH [17–19]. Theories like loop quantum gravity and string theory present modifications to Einstein's field equations [20], generally through additional terms that significantly impact black hole structure near the event horizon — where quantum effects overpower. For instance, Lewandowski et al. [21] proposed a quantum-corrected black hole model that resolves the singularity problem by halting collapse at the Planck scale Studies on the characteristics of these QCBHs have examined elements such as their silhouettes, photon rings, quasi-normal modes, and gravitational lensing [22–28]. The scarcity of rotating BH models in quantum gravity has made it difficult to test the theory

JCAP10(2025)068

using observational data. This lack of information inspired the investigation of rotating or axisymmetric extensions of spherical QCBH metrics like the one suggested by Lewandowski et al. [29, 30]. The rotating QCBH metric, derived using the Newman-Janis algorithm with parameter α, mirrors the Kerr solution and helps to test quantum gravity theories through astrophysical observations [31–37].

The study of particle dynamics around black holes (BHs) is a fundamental topic in relativistic astrophysics, providing valuable insight into the underlying physical properties of information. In this context, much research has been done in this field [38–44]. The capture and motion of both massive and massless particles in parameterized BH spacetimes have been analyzed in detail, offering a deeper analysis and illustration of their behavior in strong gravitational fields [45, 46]. Also, investigations into orbital and epicyclic frequencies in axially symmetric and stationary spacetimes have tested the stability and dynamical properties of orbits in refs. [47–50]. Also, analytical and numerical solutions to the geodesic equations play a significant role in unveiling the rich geometric structure of BH spacetimes. The pioneering work of Hagihara (see [51]) laid the foundation for analytical solutions to geodesics, which have since been further tested. Grunau and Kagramanova [52] investigated the geodesics of charged particles in the Reissner-Nordström spacetime, while Chandrasekhar in ref. [53], this study tested the particle trajectories around Schwarzschild, Reissner-Nordström, and Kerr BHs. Circular geodesics, in particular, have proven instrumental in the analysis of quasinormal modes of BH, as discussed by Nollert [54]. Also, the motion of electrically charged test particles in BH spacetimes has also been comprehensively studied, with various works focusing on their integrability and separation of motion equations, as shown and illustrated in refs. [55–58].

Epicyclic oscillations around black holes are key to understanding the dynamics of accretion disks and QPOs in microquasars and AGNs. Modeling the accretion disk that forms around the black holes can reveal shock waves that may develop on the disk and also allows for calculating LFQPOs and high-frequency quasi periodic oscillations (HFQPOs). In this way, these phenomena occurring in strong gravitational fields help to identify the consistency and differences between the results predicted by alternative gravity theories, the Kerr solution, and observations [59–72]. The parametric resonance model [73] explains QPOs in black hole disks, while relativistic effects on frequencies in non-slender tori were analyzed in [74]. Given their connection to test particle dynamics near the ISCO, accurately modeling QPO signals is crucial for diagnosing strong gravitational fields. The epicyclic motion of the test particles characterized by orbital, radial, and latitudinal frequencies has proven helpful in explaining observed HFQPOs. These observations help constrain the theoretical model parameters [75–83] and references therein. Moreover, high-precision measurements from Insight-HXMT (Hard X-ray Modulation Telescope) [84] and next-generation X-ray time-domain missions such as the Einstein Probe [85] are expected to place even more stringent constraints on the parameters of central compact objects.

BHs are among the most fascinating phenomena predicted by Einstein's relativity [86–89]. Alternatively, primordial BHs, which are just as fascinating, may exist because of variations in density during cosmic inflation or imperfections in the early universe. The determination of BH rotation in X-ray binary systems and the identification of merging binary BHs

JCAP10(2025)068

by LIGO provide evidence for the presence of BHs. These scenarios are justified by the revolutionary picture of the supermassive BH in galaxy M87 captured by the Event Horizon Telescope [90–93], as well as the use of radial velocity techniques to discover a star-BH binary system [94]. In addition, these results confirm the presence of BHs and offer a detailed explanation of the gravity interaction [95–102]. A singularity located at the core of every BH is an area with extremely high density where the usual laws of physics cease to apply because of its intense gravitational forces. Surrounding this point of infinite gravity is the event horizon, a limit where not even light can escape the powerful pull of gravity. BHs may be distinguished by some of these parameters: *(i)* mass [103], *(ii)* electric charge [104], and *(iii)* angular momentum [105]. Hawking extensively explored these qualities [106–110], presenting pioneering work on BH thermodynamics [111–116] and quantum mechanics [117–119].

The particle motion model refers to how individual particles, such as atoms, molecules, or subatomic particles, react to external forces and surroundings. Particles can illustrate different types of movement in various mediums, making this idea crucial to understanding physical systems, from basic gases to intricate quantum fields [120–125]. Studying test particles dynamically in this context provides an efficient method for illustrating BH solutions in intense gravitational fields near compact objects. Another study of classical BH solutions like Schwarzschild and Kerr BHs in strong field [126–129] and weak field [130, 131] scenarios. Nevertheless, there is significant room to explore different theories of gravity, particularly those that involve a cosmological constant and a dilaton scalar field. X-ray observations of small celestial objects have been used to investigate these alternative theories of gravity [132–134]. The ISCOs are crucial for illustrating the behavior of particles near BHs. Some studies of accretion disks constrain BH properties [135–138], while their magnetic fields significantly influence charged particles in refs. [139–142]. Another review in refs. [143–154] for explaining the interaction in the particle dynamics and spacetime around BHs.

Our study investigates the motion of test particles orbiting the rotating and axially symmetric QCBH, emphasizing how the BH's parameters influence particle motion. This quantum-corrected solution is defined by three key parameters: the BH mass M, the spin parameter a, and the deformation parameter b, which quantifies deviations from the classical Kerr BH. Analytical formulas are obtained for the radial distributions of energy and angular momentum in stable circular orbits located in the equatorial plane. In addition, utilizing the effective potential approach, we assess the stability of these paths and examine the forces influencing the particles. The stability criteria are illuminated by determining the oscillation frequencies in the radial and latitudinal directions as dependent on M, b, and a. Furthermore, we investigate inner stable circular orbits, QPOs, precession effects, periastron precession (PP) and the Lense-Thirring effect. In this context, our results show that the influence of this parameter on the BH is essential to influence the movement of particles, providing a better discussion of how matter behaves near QCBHs. In addition, we analyze QPOS effects and test how different parameters affect their frequencies and amplitudes.

This paper is organized as follows: in section 2, we present the spacetime geometry of rotating quantum-corrected black holes and derive the fundamental equations that govern particle motion. We analyze circular orbits, effective potentials, and effective forces acting on test particles. Section 3 investigates harmonic oscillations around stable circular orbits. We

JCAP10(2025)068

compute the fundamental frequencies (ν_r, ν_θ, ν_ϕ) and examine the periastron precession and Lense-Thirring effects, comparing results with classical Kerr black hole predictions. Finally, section 6 summarizes our key findings and discusses their implications for testing quantum gravity effects through astrophysical observations of black hole systems.

Throughout this paper, unless stated otherwise, geometrized units with $G = c = 1$ are used, expressing all quantities in terms of the black hole mass. As a result, the findings are applicable to both stellar-mass and supermassive black holes.

2 Rotating quantum corrected BH

We present the space-time geometry of a rotating black hole with quantum corrections, characterized by three fundamental parameters: the mass M, the rotation parameter a, and the dimensionless quantum correction parameter b. The line element of the rotating quantum-corrected black hole (QCBH) takes the form [36, 37]:

$$\begin{aligned} ds^2 = &-\left(1-\frac{2M(r)r}{\Sigma}\right)dt^2 - \frac{4aM(r)r\sin^2\theta}{\Sigma}dtd\phi \\ &+\frac{\Sigma}{\Delta}dr^2 + \Sigma d\theta^2 + \left(r^2+a^2+\frac{2a^2M(r)r\sin^2\theta}{\Sigma}\right)\sin^2\theta d\phi^2, \end{aligned} \tag{2.1}$$

where

$$\begin{aligned} \Delta &= r^2 + a^2 - 2M(r)r, \quad M(r) = M - \frac{bM^4}{2r^3}, \\ \Sigma &= r^2 + a^2\cos^2\theta. \end{aligned}$$

The metric (2.1) contains three physical parameters: the mass M sets the overall scale of the black hole, the rotation parameter a (with $0 \leq a \leq M$) determines the angular momentum, and the quantum correction parameter b quantifies deviations from the Kerr black hole. Several critical limits emerge from this solution: when $b = 0$, the metric reduces exactly to the Kerr solution. We recover the Schwarzschild metric for $a = 0$ and $b = 0$. The case $a = 0$ with $b \neq 0$ corresponds to a spherically symmetric quantum-corrected black hole.

Quantum corrections ($b \neq 0$) considerably alter particle dynamics relative to conventional Kerr black holes, primarily through outward shifts of ISCO positions of up to 25% for common b values and characteristic changes in epicyclic frequency ratios. The accretion disk simulations demonstrate similar changes in QPO signals, with frequency profiles that may identify QCBHs from normal Kerr black holes in observational data from sources such as GRS 1915+105 and GRO J1655-40. We develop a complete framework for connecting these theoretical predictions to observable values, while also carefully discussing the scale gap between quantum corrections and classical black hole properties. That b is a phenomenological parameter that encodes quantum corrections to the classical Kerr metric. This is motivated by effective models in loop quantum gravity (LQG) and related techniques [155, 156]. In LQG, such parameters are frequently related to the smallest area gap or bounce surface, which replaces the classical singularity with a Planck-scale finite-curvature region. Our model does not explicitly incorporate a bounce, but b alters the mass function $M(r) = M - bM^4/(2r^3)$,

JCAP10(2025)068

introducing quantum corrections that dominate at tiny r. The locations of the horizon are the roots of the equation $\Delta(r) = 0$, which becomes:

$$r^2 + a^2 - 2\left(M - \frac{bM^4}{2r^3}\right) r = 0. \tag{2.2}$$

This quintic equation governs the inner and outer horizons, with the outer solution representing the event horizon. The quantum correction parameter b modifies the horizon radii compared to the classical Kerr case, with the correction term becoming significant at small radii where quantum effects are expected to dominate.

2.1 Orbital dynamics around rotating QCBHs

The motion of neutral particles in the quantum-corrected spacetime is governed by the Hamiltonian formulation [157–159]. The relativistic Hamiltonian takes the form:

$$H = \frac{1}{2} g^{\alpha\beta} p_\alpha p_\beta + \frac{1}{2} m^2, \tag{2.3}$$

where m is the particle mass, $p^\gamma = m u^\gamma$ the four-momentum, $u^\gamma = dx^\gamma/d\tau$ the four-velocity, and τ the proper time. The corresponding Hamilton's equations [157–159] are:

$$\frac{dx^\gamma}{d\zeta} = m u^\gamma = \frac{\partial H}{\partial p_\gamma}, \quad \frac{dp_\gamma}{d\zeta} = -\frac{\partial H}{\partial x^\gamma}, \tag{2.4}$$

with $\zeta = \tau/m$ being an affine parameter. The spacetime symmetries yield two conserved quantities [157–159]:

$$\frac{p_t}{m} = g_{tt} u^t + g_{t\phi} u^\phi = -\mathcal{E}, \quad \frac{p_\phi}{m} = g_{\phi\phi} u^\phi + g_{t\phi} u^t = \mathcal{L}, \tag{2.5}$$

where $\mathcal{E} = E/m$ denotes the specific energy, which is a dimensionless quantity in geometrized units, and $\mathcal{L} = L/m$ is the specific angular momentum of the test particle. For the considered rotating QCBH, the Hamiltonian takes the following form:

$$H = \frac{b^2 p_r^2 + b H_2 r^2 + H_3 r^4}{2r^4 \left(b + H_1 r^2\right)}, \tag{2.6}$$

where

$$\begin{aligned}
H_1 &= a^2 + (r-2)r, \\
H_2 &= a^2\left(\mathcal{E}^2 + 2p_r^2\right) - 2a\mathcal{E}\mathcal{L} + \mathcal{L}^2 + p_\theta^2 + 2p_r^2 r^2 - 4, p_r^2 r + r^2, \\
H_3 &= a^4 p_r^2 + a^2\left(r\left(-\left(\mathcal{E}^2(r+2)\right) + 2p_r^2(r-2) + r\right) + p_\theta^2\right) + 4a\mathcal{E}\mathcal{L}r \\
&\quad + r\left(r\left(r\left(\mathcal{E}^2(-r) + r - 2\right) + p_r^2(r-2)^2\right) + \mathcal{L}^2(r-2) + p_\theta^2(r-2)\right)
\end{aligned}$$

The specific energy and specific angular momentum of particles around rotating QCBHs are calculated as:

$$\mathcal{E} = \frac{a^2\left(2br - r^4\right) - \mathcal{E}_3\mathcal{E}_2 a + br^3 + (r-2)r^6}{\sqrt{\mathcal{E}_1} r^2\left(a^2\left(2b - r^3\right) + r^6\right)}, \tag{2.7}$$

$$\mathcal{L} = \frac{a^3\left(2br - r^4\right) + 3ar^3\left(b - r^3\right) + \mathcal{E}_2 r^6 + \mathcal{E}_5}{\sqrt{\mathcal{E}_1} r^2\left(a^2\left(2b - r^3\right) + r^6\right)}, \tag{2.8}$$

JCAP10(2025)068

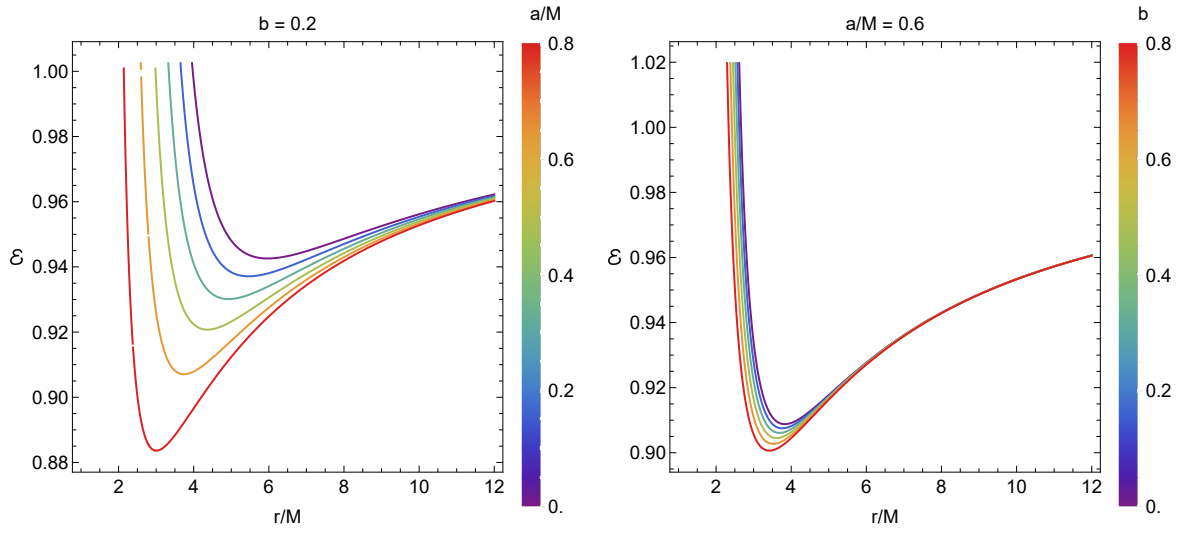

Figure 1. Graphical evolution of energy of particles encircling the rotating QCBHs.

$$
\begin{aligned}
\mathcal{E}_1 &= \frac{2a^3 r\left(r^3-2b\right)^{3/2}+3br^6+(r-3)r^9+\mathcal{E}_4}{\left(a^2\left(2b-r^3\right)+r^6\right)^2},\\
\mathcal{E}_2 &= \sqrt{r^3-2b},\quad \mathcal{E}_3 = b-2r^3,\\
\mathcal{E}_4 &= 6\mathcal{E}_2 a r^3\left(r^3-b\right)-3a^2\left(2b^2-b(2r+3)r^3+(r+1)r^6\right),\\
\mathcal{E}_5 &= \mathcal{E}_2 a^2\left(r^3(r+2)-b\right)
\end{aligned}
$$

The orbital energy characteristics of the test particles around the rotating QCBH are shown in figure 1. The left panels demonstrate the dependence on the spin parameter a, revealing that the particle energy decreases monotonically with increasing a for the fixed radial coordinate r. This behavior reflects the enhanced frame-dragging effects in rapidly rotating black holes. The right panels illustrate the influence of the quantum correction parameter b, showing that larger quantum corrections correspond to systematically higher orbital energies than the classical Kerr case ($b = 0$). In particular, the energy difference between the QCBH and Kerr solutions becomes most pronounced in the strong-field region ($r \lesssim 10M$), suggesting that quantum corrections significantly modify the structure of the potential well near the event horizon.

A comparative analysis reveals two key features: for given (r, a) values, quantum-corrected spacetimes consistently yield higher particle energies than their classical Kerr counterparts. The energy reduction rate with increasing a is steeper for larger values of b, indicating an interplay between rotational and quantum-gravitational effects. The angular momentum distribution, shown in figure 2, exhibits complementary behavior. The left panels demonstrate that increasing the spin parameter a leads to a lower specific angular momentum $\mathcal{L}$ at a fixed radius, with the reduction being most dramatic for $r \lesssim 6M$. The right panels reveal that quantum corrections (parameterized by b) similarly suppress the required angular momentum for circular orbits, although with characteristically different radial dependence. Three crucial trends emerge: a and b parameters show an inverse relationship with $\mathcal{L}$, with the spin parameter a having more pronounced effects in the strong-field regime. The

JCAP10(2025)068

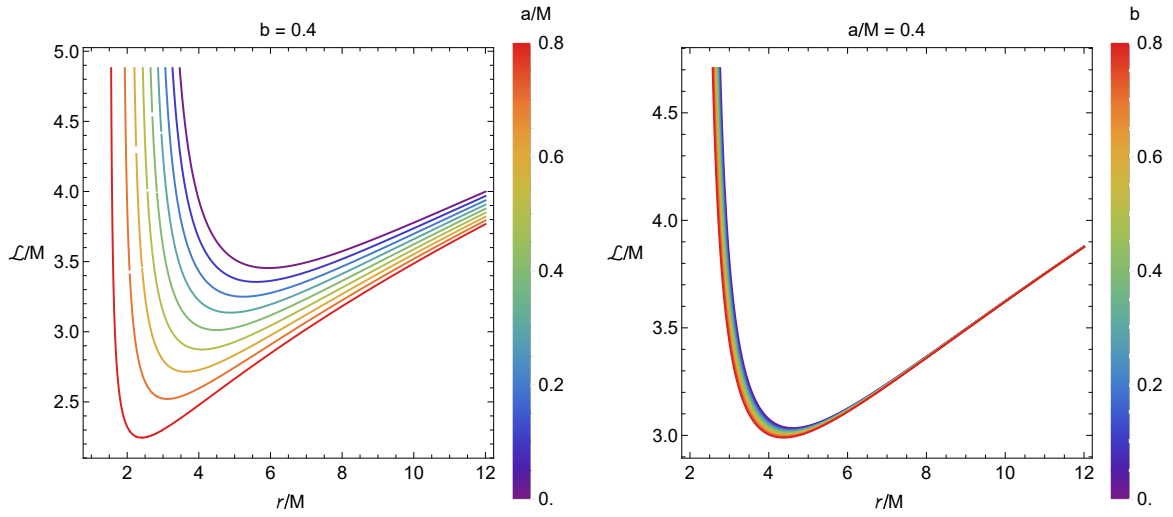

Figure 2. Graphical evolution of angular momentum of particles encircling the rotating QCBHs.

angular momentum increases monotonically with the radial distance r, approaching the classical Keplerian limit ($\mathcal{L} \propto \sqrt{Mr}$) at large distances. Quantum-corrected spacetimes require a systematically higher angular momentum than Kerr black holes at equivalent radii, particularly in the $3M < r < 10M$ range.

These energy and angular momentum characteristics directly affect accretion disk physics, as they influence the location of the ISCO, the efficiency of energy extraction mechanisms, and the spectral signatures of disk emission. The observed deviations from Kerr predictions suggest potentially observable signatures of quantum corrections in astrophysical black hole systems.

2.2 Effective potential

The effective potential formalism for particle motion in curved space-time arises naturally from the normalization condition $g_{\nu\sigma}u^{\nu}u^{\sigma} = -1$ [160, 161]. This yields the following general expression:

$$V_{\text{eff}}(r,\theta) = g_{rr}\,\dot{r}^2 + g_{\theta\theta}\,\dot{\theta}^2, \tag{2.9}$$

where $\dot{r} = dr/d\tau$ and $\dot{\theta} = d\theta/d\tau$ are proper time derivatives. The potential can be expressed in terms of metric components and constants of motion as [38, 162]:

$$V_{\text{eff}}(r,\theta) = \frac{\mathcal{E}^2 g_{\phi\phi} + 2\mathcal{E}\mathcal{L}g_{t\phi} + \mathcal{L}^2 g_{tt}}{g_{t\phi}^2 - g_{tt}g_{\phi\phi}} - 1. \tag{2.10}$$

For the space-time geometry considered here, the explicit form becomes [163, 164]:

$$V_{\text{eff}}(r,\theta) = \frac{a^2 r^3\sqrt{V_1} - a\mathcal{L}\left(b - 2r^3\right) + r\sqrt{V_1}V_2}{a^2\left(r^3(r+2) - b\right) + r^6}, \tag{2.11}$$

with the auxiliary functions:

$$V_1 = \frac{a^2\left(r^3(r+2) - b\right) + r^4\left(\mathcal{L}^2 + r^2\right)}{r^2\left(a^2 + (r-2)r\right) + b}, \tag{2.12}$$

$$V_2 = b + (r-2)r^3. \tag{2.13}$$

JCAP10(2025)068

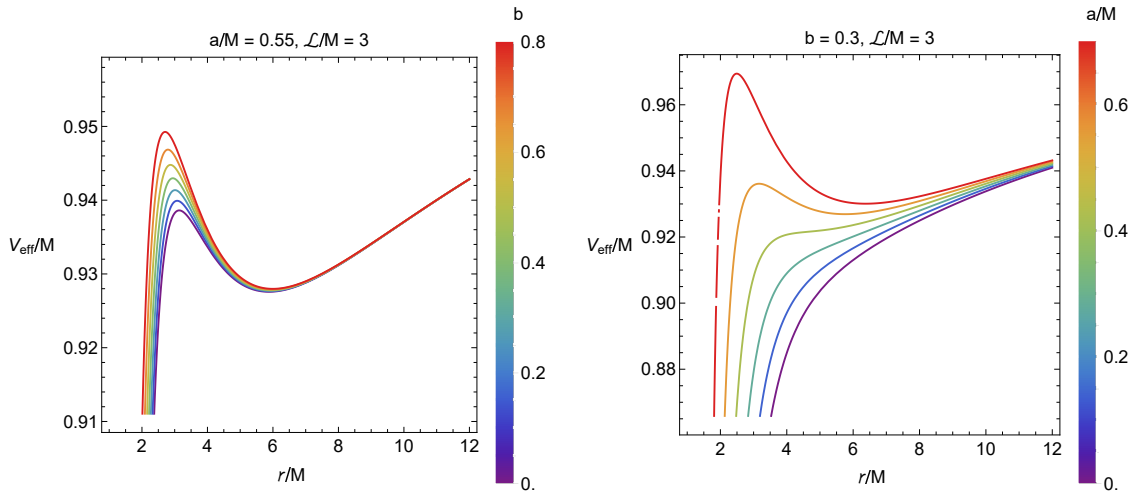

Figure 3. Graphical evolution of the effective potential of particles around rotating QCBHs.

This potential is beneficial for analyzing bound orbits and stability conditions without solving the full equations of motion [165, 166]. In the equatorial plane ($\theta = \pi/2$), circular orbits satisfy:

$$V_{\text{eff}}(r) = 0, \quad \frac{\partial V_{\text{eff}}(r)}{\partial r} = 0. \tag{2.14}$$

These conditions are fundamental for determining the ISCO and other characteristic radii [167]. The extrema of the effective potential $V_{\text{eff}}(r)$ identify circular orbits, with minima corresponding to stable configurations and maxima to unstable ones. Although Newtonian gravity predicts a fixed ISCO radius independent of angular momentum $\mathcal{L}$, relativistic systems exhibit orbital positions dependent on $\mathcal{L}$ due to additional degrees of freedom [38].

For Schwarzschild black holes, the effective potential displays two extremal points for each angular momentum value, as shown in figure 3. The ISCO location emerges from solving the simultaneous conditions:

$$\frac{\partial V_{\text{eff}}}{\partial r} = 0, \quad \frac{\partial^2 V_{\text{eff}}}{\partial r^2} \geq 0. \tag{2.15}$$

Orbital stability is critically dependent on the spin parameter a and the deformation parameter b. As either parameter increases, the region of stable orbits contracts significantly. Notably, quantum-corrected black holes (QCBHs) develop shallower potential minima near the horizon compared to their Kerr counterparts at identical spins [163], with Kerr solutions exhibiting V_{eff} minima at smaller radii. This behavior reflects how quantum corrections ($b \neq 0$) modify the space-time geometry near the event horizon.

2.3 Effective force

The radial effective force governing particle dynamics,

$$F = -\frac{1}{2}\frac{dV_{\text{eff}}}{dr}, \tag{2.16}$$

JCAP10(2025)068

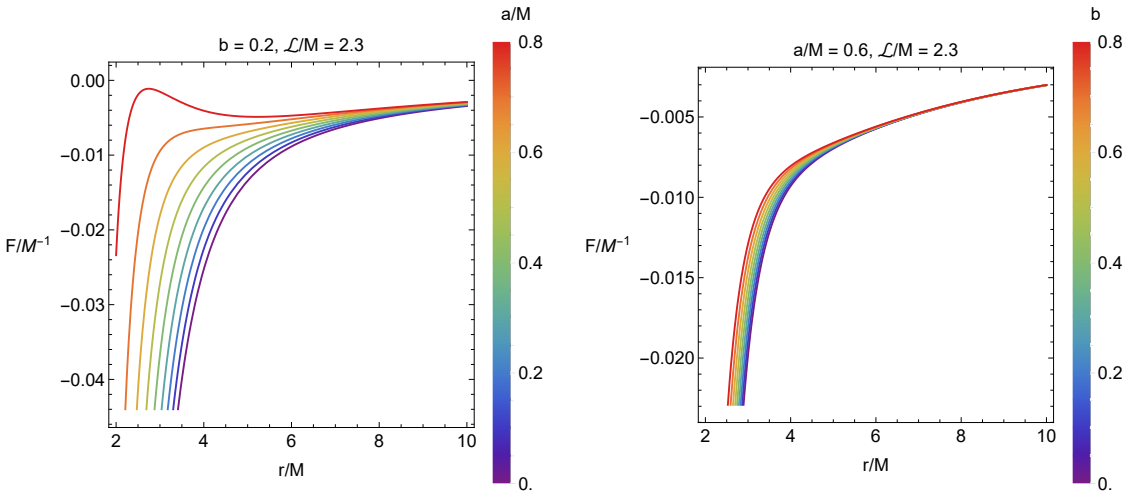

Figure 4. Graphical evolution of effective force for particles moving around rotating QCBHs.

exhibits a strong dependence on both the quantum correction parameter b and the spin parameter a, as shown in figure 4. The force magnitude increases monotonically with both parameters, transitioning from weakly attractive at small a, b to strongly repulsive at larger values. Notably, quantum-corrected black holes generate consistently stronger forces than their Kerr counterparts with equivalent spin parameters, revealing how quantum gravitational effects modify the near-horizon geometry.

3 Analyzing harmonic oscillations in the context of circular orbital motion

We consider small perturbations about stable circular orbits in the equatorial plane to analyze the oscillatory dynamics of neutral particles. When displaced from equilibrium, a test particle executes epicyclic motion, a superposition of radial and vertical harmonic oscillations. The fundamental frequencies of these oscillations, as measured by a comoving observer, are determined by the curvature of the effective potential and given by [157–159]

$$\omega_r^2 = \frac{-1}{2\,g_{rr}} \frac{\partial^2 V_{\text{eff}}(r,\theta)}{\partial r^2}, \tag{3.1}$$

$$\omega_\theta^2 = \frac{-1}{2\,g_{\theta\theta}} \frac{\partial^2 V_{\text{eff}}(r,\theta)}{\partial \theta^2}, \tag{3.2}$$

$$\omega_\phi = \frac{d\phi}{d\tau}. \tag{3.3}$$

Analyzing fundamental frequencies (ω_r, ω_θ, ω_ϕ) and their ratios reveal crucial insights into the geometry of epicyclic motions around stable circular orbits. In Newtonian gravity, the frequency degeneracy ($\omega_r = \omega_\theta = \omega_\phi$) produces simple elliptical orbits around spherical masses. However, Schwarzschild black holes break this degeneracy, establishing the hierarchy $\omega_r < \omega_\theta = \omega_\phi$. This frequency splitting generates two distinct relativistic effects: (1) a periapsis advance governed by $\omega_\phi - \omega_r$ and (2) an orbital plane precession determined by $\omega_\phi - \omega_\theta$, which becomes increasingly pronounced as particles approach the black hole.

JCAP10(2025)068

3.1 Frequencies measured by far observer

The locally measured angular frequencies ω_α (given in eqs. (3.1)–(3.3)) relate to those observed at infinity Ω_α through the redshift transformation [157–159]

$$\Omega_\alpha = \omega_\alpha \left(\frac{d\tau}{dt}\right), \tag{3.4}$$

where the redshift factor is determined by the space-time metric:

$$\frac{dt}{d\tau} = -\frac{E g_{\phi\phi} + L g_{t\phi}}{g_{tt} g_{\phi\phi} - g_{t\phi}^2}. \tag{3.5}$$

For a distant observer measuring oscillation frequencies in physical units, we convert to dimensionless form using the characteristic scale c^3/GM, yielding:

$$\nu_j = \frac{1}{2\pi}\left(\frac{c^3}{GM}\right)\Omega_j \quad [\text{Hz}]. \tag{3.6}$$

Here, $j \in \{r, \theta, \phi\}$, and Ω_r, Ω_θ, and Ω_ϕ denote angular frequencies, as observed by a distant observer, for the radial, latitudinal, and axial components, respectively. For a rotating QCBH, the expressions for Ω_α are given by:

$$\Omega_r^2 = \frac{a^4\Omega_3 + a^2\Omega_2 - 2a\mathcal{E}\mathcal{L}\Omega_4 + 3b^3\mathcal{L}^2 + \Omega_5}{\Omega_1}, \tag{3.7}$$

$$\Omega_\theta^2 = \frac{\Omega_6\left(b + H_1 r^2\right)}{r^2\left(a^2\mathcal{E}\left(r^3(r+2) - b\right) + \mathcal{E}_3 a\mathcal{L} + \mathcal{E}r^6\right)^2}, \tag{3.8}$$

$$\Omega_\phi = \frac{2ab - ar^3 + \mathcal{E}_2 r^3}{a^2\left(2b - r^3\right) + r^6}, \tag{3.9}$$

where

$$\begin{aligned}
\Omega_1 &= r^4\left(a^2\mathcal{E}\left(r^3(r+2) - b\right) + \mathcal{E}_3 a\mathcal{L} + \mathcal{E}r^6\right)^2,\\
\Omega_2 &= 3b^3\mathcal{E}^2 + b^2r^2\left(\mathcal{E}^2 r(7r-18) + 9\mathcal{L}^2\right) + 2br^5\left(\mathcal{E}^2 r\left(15r^2 - 32r + 18\right) + 3\mathcal{L}^2(4r-7)\right)\\
&\quad - \left(r^8\left(2\mathcal{E}^2 r\left(3r^2 - 14r + 12\right) + \mathcal{L}^2\left(r^2 + 6r - 12\right)\right)\right),\\
\Omega_3 &= 9b^2\mathcal{E}^2r^2 + 2br^4\left(3\mathcal{E}^2 r(5r-7) + 5\mathcal{L}^2\right) - 2r^7\left(3\mathcal{E}^2(r-2)r + \mathcal{L}^2\right),\\
\Omega_4 &= 3b^3 + 2b^2(4r-9)r^3 + b\left(21r^2 - 50r + 36\right)r^6 - 4\left(3r^2 - 8r + 6\right)r^9,\\
\Omega_5 &= -2a^6\mathcal{E}^2r^4\left(r^3 - 5b\right) + 4a^5\mathcal{E}\mathcal{L}r^4\left(r^3 - 5b\right)\\
&\quad -6a^3\mathcal{E}\mathcal{L}r^2\left(3b^2 + b(9r-14)r^3 - 2(r-2)r^6\right) - 6b^2\mathcal{E}^2r^6\\
&\quad +9b^2\mathcal{L}^2(r-2)r^3 + 2b\mathcal{E}^2(5r-3)r^9 + 9b\mathcal{L}^2(r-2)^2r^6 + r^9\left(3\mathcal{L}^2(r-2)^3 - 2\mathcal{E}^2r^4\right),\\
\Omega_6 &= -\mathcal{E}_3a^4\mathcal{E}^2 + 2\mathcal{E}_3a^3\mathcal{E}\mathcal{L} + a^2\left(2r^3 - b\right)\left(\mathcal{E}^2r^2 + \mathcal{L}^2\right) + \mathcal{L}^2r^2V_2
\end{aligned}$$

Figure 5 presents the radial profiles of epicyclic frequencies ν_j for neutral particles orbiting a rotating QCBH, demonstrating their dependence on the spin parameter a and quantum correction b as measured by a distant observer. In the non-rotating case ($a = 0$), the radial

JCAP10(2025)068

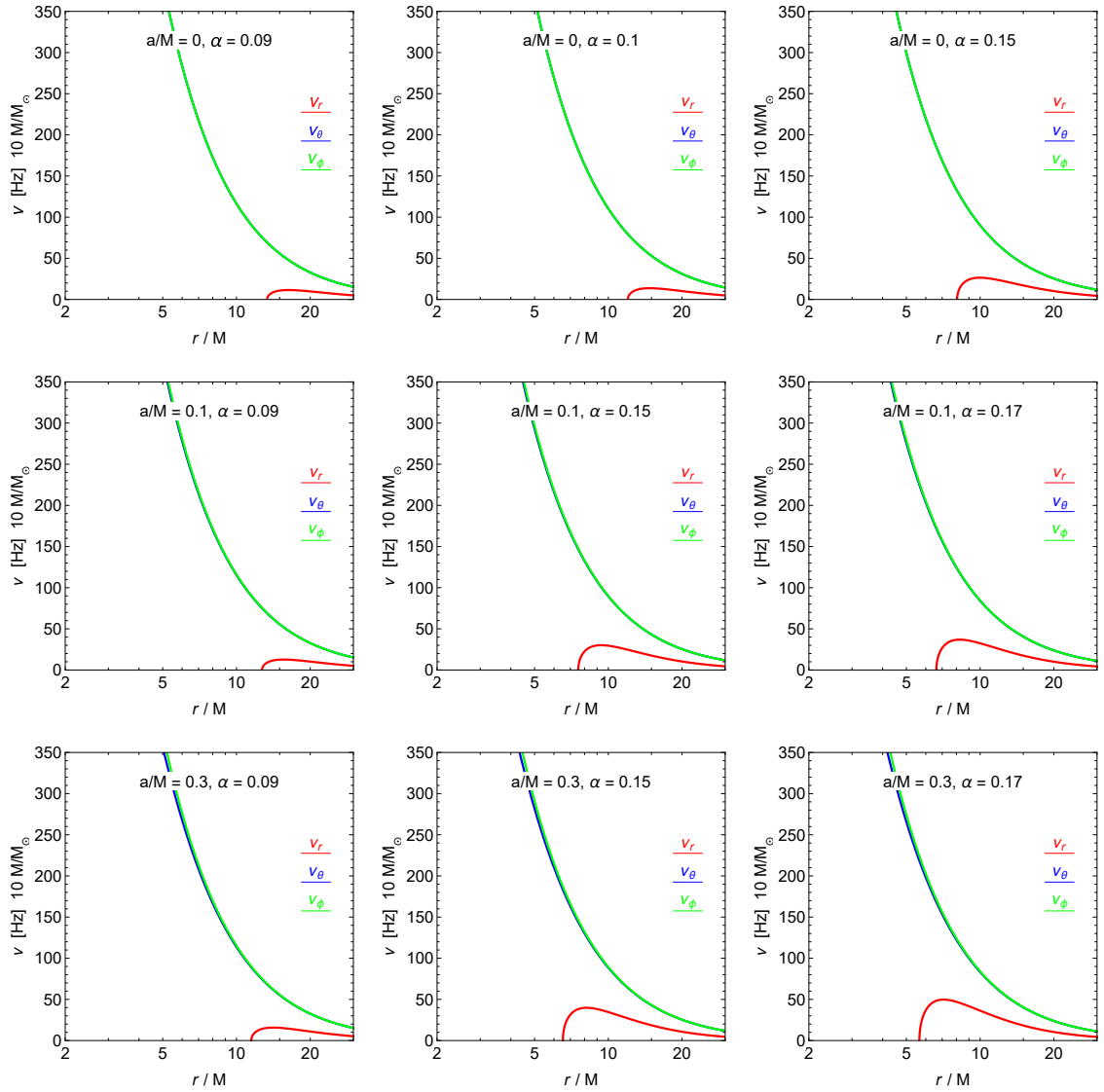

Figure 5. Graphical evolution of fundamental frequencies of particles moving around rotating QCBHs.

and vertical frequency profiles degenerate, as evident in the plots' top row. Introducing rotation ($a > 0$) or quantum corrections ($b > 0$) breaks this degeneracy. Both parameters cause the radial frequency peak to shift inward toward smaller radii, with the effect being more pronounced for QCBHs than for Kerr black holes with identical spin. This inward migration of frequency profiles reveals how quantum corrections enhance relativistic effects near the horizon, modifying the orbital dynamics compared to classical Kerr predictions.

3.2 Periapsis and lense-thirring in quantum-corrected spacetime

We analyze the Lense-Thirring precession (LTP) and periapsis precession for neutral test particles in slightly inclined orbits ($\theta \approx \pi/2$) around a rotating quantum-corrected black hole (QCBH). The particle's epicyclic motion with radial frequency Ω_r enables a precise measurement of these relativistic effects.

JCAP10(2025)068

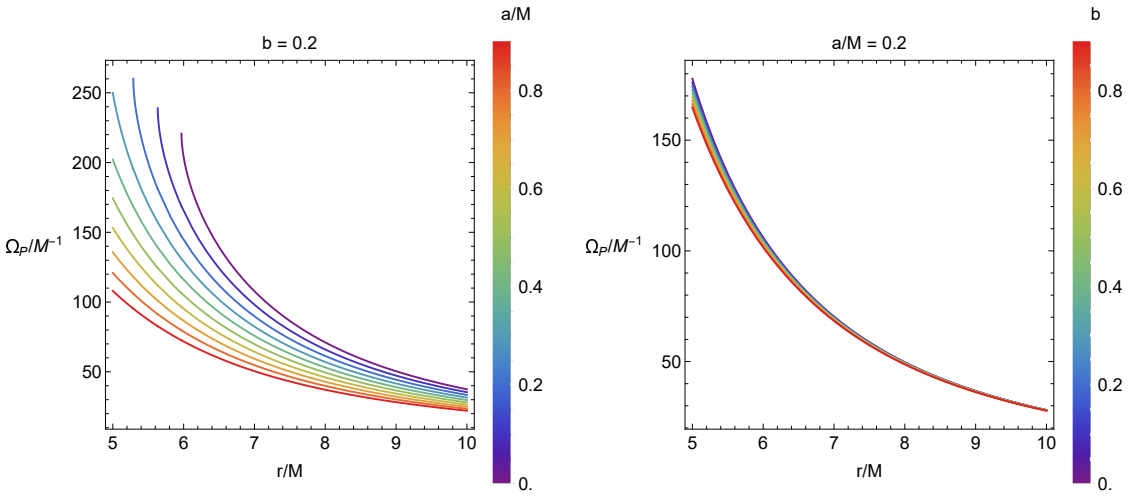

Figure 6. Graphical evolution of periastron frequency of particles around rotating QCBHs.

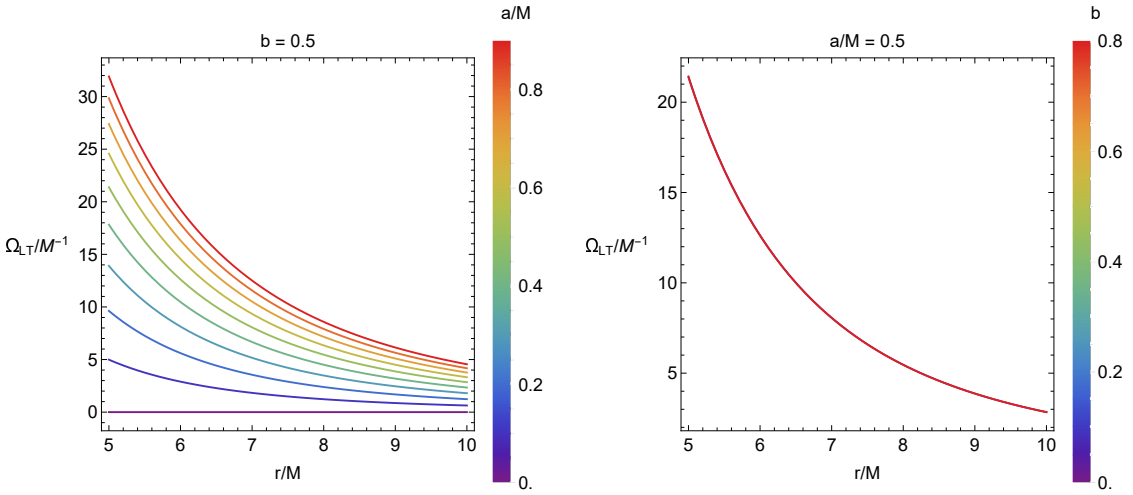

Figure 7. Graphical evolution of Lense-Thirring precession frequency around rotating QCBHs.

The precession frequencies are defined as [157–159]:

$$\Omega_P = \Omega_\phi - \Omega_r \quad \text{(periapsis precession)} \tag{3.10}$$

$$\Omega_{LT} = \Omega_\phi - \Omega_\theta \quad \text{(Lense-Thirring precession)} \tag{3.11}$$

These effects fundamentally differ from Newtonian gravity, where $\Omega_r = \Omega_\phi$. The precession of the periapsis Ω_P, visualized in figure 6, describes the orbital advance in the plane, while Ω_{LT} (nonzero only when $a \neq 0$) quantifies the precession of the nodal plane from the drag of the frame.

For non-rotating black holes ($a = 0$), $\Omega_\theta = \Omega_\phi$ eliminates LTP while preserving periapsis precession. As shown in figure 7, increasing the spin parameter a produces two competing effects: it enhances Ω_{LT} through stronger frame drag while reducing Ω_P. The quantum correction parameter b shows a markedly different influence — while it negligibly affects Ω_{LT}, it significantly modifies the Ω_P profiles compared to classical Kerr solutions.

JCAP10(2025)068

4 Comparison of test particle dynamics and numerical accretion flow around QCBH

Here, we compare the motion of the test particle in the strong gravitational field around the QCBH with the behavior of the accretion disk formed in the same strong gravitational region, i.e., very close to the horizon of the QCBH. By doing so, we analyze the physical implications introduced by the b in each case. To achieve this, we numerically solve the general relativistic hydrodynamic equations (GRH), modeling the matter infall through Bondi-Hoyle-Lyttleton (BHL) accretion toward the black hole, and thereby simulate the formation of the accretion disk and the resulting shock cone in the equatorial plane. The boundary conditions, initial conditions, and other physical parameters used in the modeling are described in detail in [61, 65, 68].

To enable a meaningful comparison, we compute the mass accretion rate, which characterizes the behavior of matter in a strong gravitational field near the ISCO. The mass accretion rate presented in figure 8 is calculated at $r = 2.3M$, and its time evolution is shown for different values of the quantum correction parameter b. As in the rest of the paper, all the parameters in this figure are expressed in geometrized units. As shown in figure 8, the parameter b significantly alters the amount of matter falling towards the black hole. As b increases, the amount of accreted matter shows a noticeable increase. The mass accretion rate obtained from the numerical simulations is consistent with the effective potential derived from the motion of the test particle, as shown in figure 2. As is well known, a deeper effective potential allows more matter to accrete and fall toward the black hole. In figure 3, the depth of the effective potential increases with increasing b, and a similar trend is observed in the mass accretion rates obtained from the numerical simulations in figure 8. Therefore, the theoretical and numerical results agree well.

However, as also shown in figure 8, it exhibits a quasi periodic behavior after the accretion disk reaches a steady state. This behavior indicates the formation of QPOs in the strong gravitational field. As also seen in figure 8, the increase in b has caused a slight decrease in the amplitude of the oscillations. In this case, the resulting QPOs are expected to have lower amplitudes and potentially altered QPO frequencies. As a result, the quantum correction parameter b has significantly impacted the physical phenomena that occur around QCBH. Since these effects lead to observable changes, this type of model — incorporating deviations from the Kerr black hole geometry — could potentially explain observational data that cannot be fully accounted for using the standard Kerr geometry alone.

As mentioned earlier, the QPOs seen in the mass accretion rate profiles shown in figure 8 indicate the presence of QPO frequencies. To calculate the resulting QPO frequencies, we performed a Power Spectral Density (PSD) analysis using the mass accretion rate for both the Kerr black hole and the QCBH with $b = 0.2$.

The results of this analysis, presented in figure 9, show that the PSD amplitudes in the Kerr case are slightly higher than those in the QCBH case. PSD amplitudes are a key factor that affects whether QPO frequencies can be observed. In the Kerr case, the lowest frequency occurs at 3.4 Hz, whereas in the QCBH case, these frequencies vary within the range of 2.2–5.5 Hz. Previous studies and observational results indicate that these low frequencies arise due to space-time frame-dragging effects caused by black hole spin. They

JCAP10(2025)068

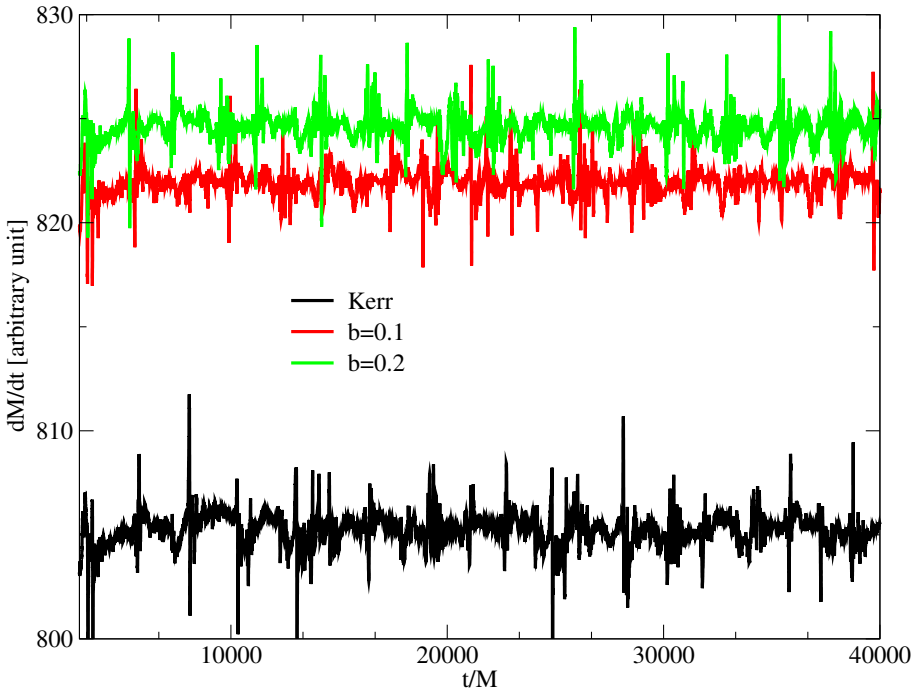

Figure 8. The time evolution of the mass accretion rate in the strong gravitational field around the QCBH with a spin parameter $a/M = 0.9$ is shown for different values of the quantum correction parameter b. It is observed that as b increases, the mass accretion rate also increases. Additionally, after the accretion disk reaches a steady state, it exhibits oscillatory behaviour around a certain value.

JCAP10(2025)068

are known as Lense-Thirring frequencies [67]. These frequencies are nearly identical in both cases, indicating that the quantum correction parameter b does not significantly alter this specific QPO component. This result is also supported by the analytical solution shown in figure 7, which is based on the motion of a test particle around the QCBH. Section 5 provides a detailed discussion regarding the observational, numerical, and theoretical implications of QPO frequencies that arise due to the Lense-Thirring effect.

In figure 9, additional peaks are observed in both models that result from the trapping of pressure modes within the accretion disk and their non-linear couplings. However, the dominant QPO peak shifts from 8.8 Hz (Kerr) to 10.1 Hz (QCBH) when the quantum correction parameter b is introduced. This shift arises entirely from the modification of the gravitational potential around the QCBH by the parameter b. This effect is also shown for the test particle case in figure 3.

In conclusion, the gravitational potential, turbulence, and instabilities around the QCBH are influenced by the quantum correction parameter b, which leads to modifying the spacetime structure in the strong gravity region. It causes a shift in the ISCO location and a change in the depth of the effective potential, both of which result in changes in the QPO frequencies. These changes are clearly demonstrated in both the test particle model and the numerical simulations. Moreover, they also affect the observability of QPOs. Lower QPO amplitudes and shifted frequencies in the QCBH model suggest that specific observed QPO signals

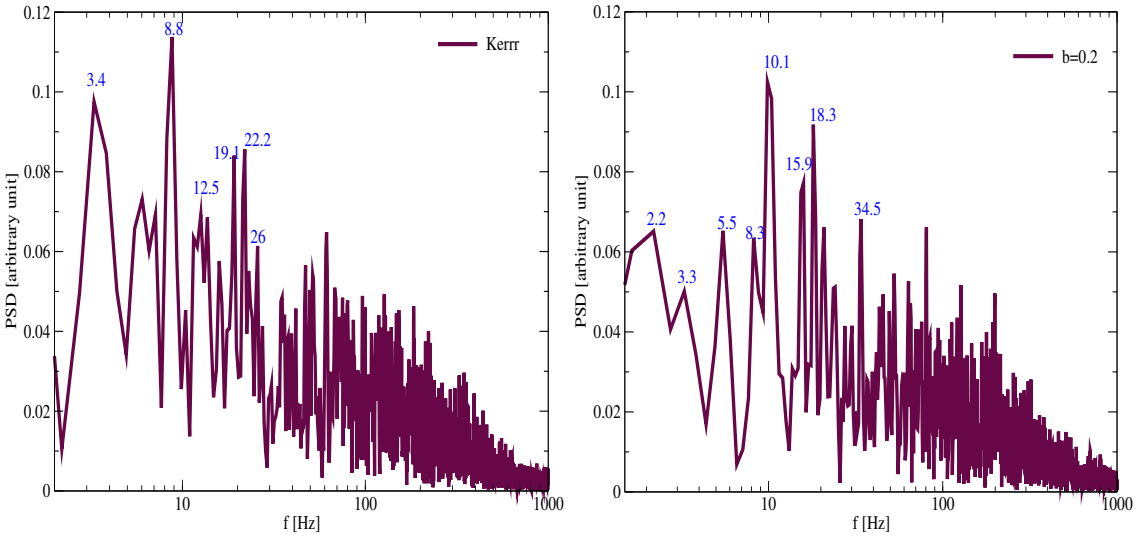

Figure 9. PSD profiles as a function of frequency for a black hole with $M = 10\,M_{\odot}$ are shown for both the Kerr and QCBH cases. In the QCBH scenario, the quantum correction parameter is set to $b = 0.2$. While QPO frequencies appear in both cases, the Kerr black hole exhibits a higher peak PSD amplitude, indicating stronger dominant oscillatory modes. In contrast, the QCBH case shows a redistribution of spectral power toward lower frequencies, resulting in a broader and more flattened PSD profile.

in black hole X-ray binaries may not be fully explained by Kerr spacetime alone. The QCBH framework could provide new information on unexplained QPO behaviors, such as weak or shifted QPOs.

5 QPO formation via lense-thirring precession: a comparative study of test particle and accretion disk models

Analyzing QPOs around black holes will not only help us understand the phenomena occurring in strong gravitational fields. Still, it will also enable us to reveal the physical properties of the black hole itself. Comparison of the QPO frequencies observed in X-ray data from specific sources with those obtained through theoretical and numerical calculations will significantly contribute to the literature. In this context, this study aims to contribute to the literature by examining the similarities and differences between the QPOs that arise due to the Lense-Thirring effect around QCBHs calculated using test particles — and the QPOs obtained from accretion disk models based on both the Kerr metric and alternative gravity theories.

The particle model investigates the geodesic motion of a test particle around the QCBH. Therefore, the calculations do not include non-gravitational forces, such as pressure. From the motion of the test particle, the orbital, radial, and vertical frequencies are determined in the strong gravitational field region of the QCBH ($r < 10M$) are determined. Based on these frequencies, the variation of the precession frequency caused by the Lense-Thirring effect is analyzed with respect to the black hole spin and quantum deformation parameters. On the other hand, in the disk model, plasma structures formed around black holes through BHL accretion are modeled in different gravity theories, and the resulting QPO behavior

JCAP10(2025)068

is explored [62, 64, 65, 67]. Numerical analyses reveal how QPOs resulting from the Lense-Thirring effect are influenced by physical factors such as the black hole's spin parameter, the physical characteristics of the accretion mechanism, and the shock waves that form. In the disk model, the QPO frequencies obtained give the same value at any point within the strong gravitational field. In contrast, in the particle model, these frequencies vary depending on the radial coordinate r.

Theoretically, it is known that the QPOs calculated in the test particle model originate from modes trapped within the potential well near the black hole horizon. Of course, the potential well is influenced by the black hole spin parameter and the quantum deformation parameter. These factors lead to variations in QPO frequencies. In contrast, in the disk model, it is understood that these QPOs arise not only due to the black hole's spin parameter but also from the trapping of modes by shock waves formed on the disk — and even from their nonlinear couplings. The modes trapped in the disk model are identified as $g-$modes and $p-$modes. As seen in figure 6, the periapsis precession frequency is affected by the black hole's spin and the quantum deformation parameter. In contrast, as shown in figure 7, it is demonstrated that the Lense-Thirring frequency is influenced solely by the black hole spin parameter. However, in the disk model, similar to the test particle model, the effect of the black hole spin parameter is visible (see figures 3 and 7 in [168], figures 2 and 5 in [68], and figure 16 in [59]). In addition, it has been numerically shown under different gravity theories that the shock waves occurring in the strong gravitational field, the nature of the accretion mechanism and its initial conditions, and the suppression or enhancement of modes by pressure forces influence the amplitude of QPOs arising from the Lense-Thirring effect, either increasing or decreasing it [59, 61, 62, 64, 66].

It is well known that LFQPOs generally arise from the Lense-Thirring precession effect. This effect is entirely a consequence of spacetime being warped in the strong gravitational field near the event horizon of a spinning black hole. The LFQPO frequencies observed in different sources from various observational datasets, the frequencies we calculate based on the motion of a test particle in this study, and those obtained from our numerical solutions of the GRH using an accretion disk model in the strong gravity regime [168] are listed in table 1. In this study, we find that the Lense-Thirring precession frequency derived analytically from the precessional motion of a test particle around the black hole is in strong agreement with the QPO frequencies resulting from our GRH-based numerical accretion disk simulations, which model the interaction between matter and the black hole in a strong gravitational field. Moreover, the theoretical and numerical results agree with the observational data. As observed in the analytically derived test particle models and the numerically modelled accretion disk, no LFQPOs are generated for a non-rotating black hole (i.e. for spin parameter $a = 0$). This result serves as a key confirmation that the observed LFQPOs originate from Lense-Thirring precession. Since a non-spinning black hole does not induce spacetime frame dragging, these oscillations do not occur in such cases. Furthermore, our accretion disk model shows that even in the presence of a rapidly spinning black hole, if the infalling matter exhibits purely sonic behaviour, LFQPOs are not generated. It is also observed that the LFQPO frequency varies depending on whether the accreting matter is subsonic or supersonic. This finding suggests that the behaviour of matter near the black hole, shaped by the curvature of spacetime, directly impacts the generation of QPOs. Notably, QPOs that might be predicted

JCAP10(2025)068

Source	Mass ($M_\odot$)	a/M	LFQPOs (Hz)	$\mathcal{M}$
Observation				
$GRS1915+105$ [169–172]	12–18	0.98	1–10	–
$GROJ1655-40$ [173, 174]	6.3	0.3–0.9	0.1–10	–
$XTEJ1550-564$ [175]	9.1	0.34–0.55	0.1–10	–
$H1743-322$ [176]	8–10	0.2–0.48	0.1–10	–
Accretion Disk [168]				
–	10	0.9	No	1
–	10	0.9	6.6	2
–	10	0.9	1.5	3
–	10	0.9	7.4	4
–	10	0.5	4	2
–	10	0.0	No	2
Test Particle ($b=0.2$)				
–	10	0.9	5.1	–
–	10	0.5	3.02	–
–	10	0.0	No	–

Table 1. Comparison of LFQPOs obtained from observational results of different sources with QPOs derived from numerical simulations of the accretion disk and analytically calculated test particle QPOs. Here, a/M represents the spin parameter of the black hole, $\mathcal{M}$ denotes the Mach number of the accreting matter in the accretion disk scenario.

analytically from idealized test particle motion are not always observable, highlighting the importance of incorporating full fluid dynamics and relativistic effects in modelling.

In summary, both test particle and accretion disk models provide crucial insights into the nature of QPOs formed around black holes. These studies are essential for understanding the origin of QPOs and proposing physical mechanisms that explain the QPOs observed in the data. While the test particle model is crucial in understanding QPO behaviour and for testing relativistic orbital models, accretion disk models are valuable for uncovering the rich dynamical physical structures and exploring how they vary under Kerr and alternative gravity theories. With the accretion disk model, we reveal the fundamental modes and calculate the QPO frequencies that result from the nonlinear coupling these modes can produce. Therefore, such studies will shed light on interpreting future observational data.

6 Conclusions

This work comprehensively investigates epicyclic oscillations around rotating QCBHs, exploring how quantum corrections influence particle dynamics, accretion processes, and observable phenomena in the strong gravity regime. The key results of our study can be outlined as follows:

JCAP10(2025)068

- The quantum correction parameter b and rotation parameter a significantly modify the energy and angular momentum profiles of particles in stable circular orbits (figures 1–2). Compared to the classical Kerr solution, particles orbiting QCBHs exhibit higher energy and angular momentum values, with these differences becoming more pronounced near the event horizon.

- The effective potential analysis (figure 3) indicates that quantum corrections enhance the potential barrier, making circular orbits less stable compared to the Kerr case. This effect is particularly noticeable for larger values of b, indicating that quantum corrections impact accretion disk structure and stability (figure 8).

- The effective force experienced by test particles (figure 4) shows stronger attractive behaviour in QCBHs compared to Kerr black holes, with the force magnitude increasing with both a and b parameters, which has implications for particle capture rates and accretion processes.

- Our calculation of fundamental oscillation frequencies (figure 5) demonstrates that quantum corrections shift the radial profiles of ν_r, ν_θ, and ν_ϕ closer to the black hole. The frequency ratios, particularly the 3:2 ratio often observed in QPOs, show measurable deviations from Kerr predictions that future high-precision X-ray timing observations could potentially constrain.

- The precession effects (figures 6–7) exhibit distinct dependence on the quantum correction parameter. While the Lense-Thirring precession is primarily governed by the rotation parameter a, the periastron precession shows sensitivity to a and b, providing an additional channel to probe quantum corrections.

- The radial (ν_r), vertical (ν_θ), and orbital (ν_ϕ) frequencies (figure 5) are influenced by a and b. For non-rotating BHs ($a = 0$), ν_r and ν_θ coincide, but increasing a or b breaks this degeneracy, shifting ν_r to smaller radii — indicating tighter orbital confinement near the black hole.

- Periastron precession (Ω_P, figure 6) decreases with a, while Lense-Thirring precession (Ω_{LT}, figure 7) increases with a, highlighting how frame-dragging alters orbital planes in rotating spacetimes.

- Through numerical simulations, it has been demonstrated that the plasma structure formed due to BHL accretion of matter around the QCBH generates QPOs by trapping pressure modes, which in turn excite various modes that give rise to QPO frequencies. The numerical results reveal the presence of fundamental pressure modes and additional modes formed through their nonlinear couplings. These modes have been numerically confirmed to depend on the quantum correction parameter b strongly. Additionally, the simulations show the presence of mode frequencies arising from the Lense-Thirring effect. It has been confirmed — both in the accretion disk model and the test particle model — that this particular frequency changes only with the spin parameter of the black hole, and the influence of b on it is negligibly small.

JCAP10(2025)068

- The parameter b has a negligible impact on Ω_{LT}, suggesting that quantum corrections predominantly modify the radial dynamics rather than the spacetime rotation effects, which remain dominated by the spin parameter a. At the same time, it has been demonstrated that the Lense-Thirring frequency is consistent with the LFQPOs observed from some sources and obtained through numerical solutions of the GRH equations in strong gravitational fields, which, in turn, reinforces the validity of the studies conducted here.

These results have several important implications for astrophysical observations and theoretical studies: the modifications to orbital frequencies and precession effects suggest that quantum corrections could potentially explain certain anomalies in observed QPO spectra from microquasars and AGNs. Our frequency calculations provide concrete predictions that can be compared with data from current and future X-ray timing missions. The enhanced effective potential and force effects indicate that quantum corrections may influence the thermodynamic properties of the accretion disk and the emission properties. It could be relevant for interpreting the spectra of black holes where quantum gravity effects might be significant, such as primordial or microscopic holes in certain theories. Our work provides a framework for testing quantum gravity models through astrophysical observations. The measurable differences from Kerr predictions, particularly in the strong-field regime near the ISCO, offer potential observational signatures for quantum corrections.

Several directions for future research emerge from this work. One can extend our analysis to include charged particle dynamics and electromagnetic field effects, which would be relevant for magnetized accretion disks. Investigating resonance phenomena between different oscillation modes could enhance quantum corrections' observational signatures. More detailed models were developed to connect our particle dynamics results to actual QPO observations, including radiative transfer calculations through quantum-corrected spacetimes. Application of our framework to specific quantum gravity models to derive constraints on fundamental parameters from astrophysical data.

In conclusion, our study demonstrates that quantum corrections to black hole spacetimes can have observable consequences for particle dynamics and oscillation frequencies. Although current observational precision may not yet allow for definitive detection of these effects, next-generation X-ray timing instruments and gravitational wave detectors could provide the necessary sensitivity to test these predictions. The framework developed here is an essential step toward bridging quantum gravity theories with astrophysical observations of black holes. While the predicted effects for astrophysical black holes are negligible if b is set to its natural Planck-scale value, the framework developed here serves as an important foundation for future searches for quantum gravitational signatures. The frequency profiles and modified precession effects we discovered provide solid theoretical frameworks that could guide future high-precision X-ray timing missions. This work connects quantum gravity phenomenology with relativistic astrophysics, developing a framework that may be applied to more full quantum-gravitational models as they become available. The results highlight how careful analysis of accretion disk dynamics and QPOs can provide novel constraints on spacetime structure in the strong-field regime.

JCAP10(2025)068

Acknowledgments

The author SKM acknowledges that the Ministry of Higher Education, Research, and Innovation (MoHERI) supported this research work through the project BFP/RGP/CBS/24/203 and he also thankful to UoN administration for continuous support and encouragement for the research works. All numerical simulations were performed using the Phoenix High Performance Computing facility at the American University of the Middle East (AUM), Kuwait. S.G.G. would like to thank ANRF, India, for project No. ANRF/2021/005771.

References

[1] A. Einstein, *Die Feldgleiehungen der Gravitation*, *Sitzungsber. Königl. Preuss. Akad. Wiss. Berlin* **25** (1915) 844.

[2] C.M. Will, *The Confrontation between General Relativity and Experiment*, *Living Rev. Rel.* **17** (2014) 4 [arXiv:1403.7377] [INSPIRE].

[3] LIGO Scientific and Virgo collaborations, *Observation of Gravitational Waves from a Binary Black Hole Merger*, *Phys. Rev. Lett.* **116** (2016) 061102 [arXiv:1602.03837] [INSPIRE].

[4] K. Schwarzschild, *Über das Gravitationsfeld eines Massenpunktes nach der Einsteinsehen Theorie*, *Sitzungsber. Königl. Preuss. Akad. Wiss. Berlin* (1916) 189.

[5] Supernova Search Team collaboration, *Observational evidence from supernovae for an accelerating universe and a cosmological constant*, *Astron. J.* **116** (1998) 1009 [astro-ph/9805201] [INSPIRE].

[6] A. Einstein, *The foundation of the general theory of relativity*, *Annalen Phys.* **354** (1916) 769.

[7] A. Einstein and N. Rosen, *Two-Body Problem in General Relativity Theory*, *Phys. Rev.* **49** (1936) 404 [INSPIRE].

[8] A. Einstein and N. Rosen, *The Particle Problem in the General Theory of Relativity*, *Phys. Rev.* **48** (1935) 73 [INSPIRE].

[9] J. Plebanski and A. Krasinski, *An introduction to general relativity and cosmology*, Cambridge University Press (2006).

[10] R. d'Inverno, *Introducing Einstein's relativity*, Clarendon Press, Oxford, U.K. (1992) [INSPIRE].

[11] M.P. Hobson, G.P. Efstathiou and A.N. Lasenby, *General relativity: An introduction for physicists*, Cambridge University Press (2006) [INSPIRE].

[12] C. Liu et al., *Shadow and quasinormal modes of a rotating loop quantum black hole*, *Phys. Rev. D* **101** (2020) 084001 [*Erratum ibid.* **103** (2021) 089902] [arXiv:2003.00477] [INSPIRE].

[13] M. Afrin, S. Vagnozzi and S.G. Ghosh, *Tests of Loop Quantum Gravity from the Event Horizon Telescope Results of Sgr A**, *Astrophys. J.* **944** (2023) 149 [arXiv:2209.12584] [INSPIRE].

[14] S. Brahma, C.-Y. Chen and D.-H. Yeom, *Testing Loop Quantum Gravity from Observational Consequences of Nonsingular Rotating Black Holes*, *Phys. Rev. Lett.* **126** (2021) 181301 [arXiv:2012.08785] [INSPIRE].

[15] R. Kumar Walia, *Observational predictions of LQG motivated polymerized black holes and constraints from Sgr A* and M87**, *JCAP* **03** (2023) 029 [arXiv:2207.02106] [INSPIRE].

[16] S.U. Islam, J. Kumar, R. Kumar Walia and S.G. Ghosh, *Investigating Loop Quantum Gravity with Event Horizon Telescope Observations of the Effects of Rotating Black Holes*, *Astrophys. J.* **943** (2023) 22 [arXiv:2211.06653] [INSPIRE].

JCAP10(2025)068

[17] M. Afrin, S. Vagnozzi and S.G. Ghosh, *Tests of Loop Quantum Gravity from the Event Horizon Telescope Results of Sgr A**, *Astrophys. J.* **944** (2023) 149 [arXiv:2209.12584] [INSPIRE].

[18] J. Yang, C. Zhang and Y. Ma, *Shadow and stability of quantum-corrected black holes*, *Eur. Phys. J. C* **83** (2023) 619 [arXiv:2211.04263] [INSPIRE].

[19] B.P. Singh, R. Kumar and S.G. Ghosh, *Effect of higher dimensions on rotating black holes shadow*, *New Astron.* **99** (2023) 101945 [INSPIRE].

[20] Y. Hou, M. Guo and B. Chen, *Revisiting the shadow of braneworld black holes*, *Phys. Rev. D* **104** (2021) 024001 [arXiv:2103.04369] [INSPIRE].

[21] I. Banerjee, S. Chakraborty and S. SenGupta, *Hunting extra dimensions in the shadow of Sgr A**, *Phys. Rev. D* **106** (2022) 084051 [arXiv:2207.09003] [INSPIRE].

[22] A.S. Lemos, J.A.V. Campos and F.A. Brito, *Hunting for extra dimensions in black hole shadows*, *Phys. Rev. D* **110** (2024) 064079 [arXiv:2407.04609] [INSPIRE].

[23] T. Baker, D. Psaltis and C. Skordis, *Linking Tests of Gravity On All Scales: from the Strong-Field Regime to Cosmology*, *Astrophys. J.* **802** (2015) 63 [arXiv:1412.3455] [INSPIRE].

[24] A.E. Broderick, T. Johannsen, A. Loeb and D. Psaltis, *Testing the No-Hair Theorem with Event Horizon Telescope Observations of Sagittarius A**, *Astrophys. J.* **784** (2014) 7 [arXiv:1311.5564] [INSPIRE].

[25] M. Khodadi, A. Allahyari, S. Vagnozzi and D.F. Mota, *Black holes with scalar hair in light of the Event Horizon Telescope*, *JCAP* **09** (2020) 026 [arXiv:2005.05992] [INSPIRE].

[26] M. Khodadi, G. Lambiase and D.F. Mota, *No-hair theorem in the wake of Event Horizon Telescope*, *JCAP* **09** (2021) 028 [arXiv:2107.00834] [INSPIRE].

[27] Y. Wang et al., *Strong gravitational lensing by static black holes in effective quantum gravity*, *Eur. Phys. J. C* **85** (2025) 302 [arXiv:2410.12382] [INSPIRE].

[28] A. Alimova et al., *Impact of quantum-corrected parameter on spinning particle motion around a black hole*, *Eur. Phys. J. C* **85** (2025) 646 [INSPIRE].

[29] K. Glampedakis and G. Pappas, *Is a black hole shadow a reliable test of the no-hair theorem?*, *Phys. Rev. D* **107** (2023) 064001 [arXiv:2302.06140] [INSPIRE].

[30] J. Lewandowski, Y. Ma, J. Yang and C. Zhang, *Quantum Oppenheimer-Snyder and Swiss Cheese Models*, *Phys. Rev. Lett.* **130** (2023) 101501 [arXiv:2210.02253] [INSPIRE].

[31] H. Gong et al., *Quasinormal modes of quantum-corrected black holes*, *Phys. Rev. D* **110** (2024) 044040 [arXiv:2312.17639] [INSPIRE].

[32] J.-P. Ye et al., *Shadows and photon rings of a quantum black hole*, *Phys. Lett. B* **851** (2024) 138566 [arXiv:2312.17724] [INSPIRE].

[33] L. Zhao, M. Tang and Z. Xu, *The lensing effect of quantum-corrected black hole and parameter constraints from EHT observations*, *Eur. Phys. J. C* **84** (2024) 971 [arXiv:2403.18606] [INSPIRE].

[34] W. Liu, D. Wu and J. Wang, *Light rings and shadows of static black holes in effective quantum gravity*, *Phys. Lett. B* **858** (2024) 139052 [arXiv:2408.05569] [INSPIRE].

[35] C.-Y. Chen, *On the possible spacetime structures of rotating loop quantum black holes*, *Int. J. Geom. Meth. Mod. Phys.* **19** (2022) 2250176 [arXiv:2207.03797] [INSPIRE].

JCAP10(2025)068

[36] H. Ali, S.U. Islam and S.G. Ghosh, *Shadows and parameter estimation of rotating quantum corrected black holes and constraints from EHT observation of M87* and Sgr A**, *JHEAp* **47** (2025) 100367 [arXiv:2410.09198] [INSPIRE].

[37] A. Vachher and S.G. Ghosh, *Strong gravitational lensing by rotating quantum-corrected black holes: Insights and constraints from EHT observations of M87* and Sgr A**, *JHEAp* **45** (2025) 75 [arXiv:2410.11332] [INSPIRE].

[38] J.M. Bardeen, W.H. Press and S.A. Teukolsky, *Rotating black holes: Locally nonrotating frames, energy extraction, and scalar synchrotron radiation*, *Astrophys. J.* **178** (1972) 347 [INSPIRE].

[39] B. Mashhoon, *Stability of charged rotating black holes in the eikonal approximation*, *Phys. Rev. D* **31** (1985) 290 [INSPIRE].

[40] Z. Stuchlik and J. Schee, *Appearance of Keplerian discs orbiting Kerr superspinars*, *Class. Quant. Grav.* **27** (2010) 215017 [arXiv:1101.3569] [INSPIRE].

[41] M. Zahid, S.U. Khan and J. Ren, *Shadow cast and center of mass energy in a charged Gauss-Bonnet-AdS black hole*, *Chin. J. Phys.* **72** (2021) 575 [arXiv:2101.07673] [INSPIRE].

[42] B. Turimov, S. Usanov and Y. Khamroev, *Particles acceleration by Bocharova-Bronnikov-Melnikov-Bekenstein black hole*, *Phys. Dark Univ.* **48** (2025) 101876 [arXiv:2502.11185] [INSPIRE].

[43] Z.-L. Wang and E. Battista, *Dynamical features and shadows of quantum Schwarzschild black hole in effective field theories of gravity*, *Eur. Phys. J. C* **85** (2025) 304 [arXiv:2501.14516] [INSPIRE].

[44] E. Battista, *Quantum Schwarzschild geometry in effective field theory models of gravity*, *Phys. Rev. D* **109** (2024) 026004 [arXiv:2312.00450] [INSPIRE].

[45] A. Abdujabbarov, J. Rayimbaev, F. Atamurotov and B. Ahmedov, *Magnetized Particle Motion in γ-Spacetime in a Magnetic Field*, *Galaxies* **8** (2020) 76 [INSPIRE].

[46] O. Rahimov et al., *Charged particle dynamics in Reissner-Nordström-Tangherlini spacetime*, *Phys. Dark Univ.* **44** (2024) 101483 [INSPIRE].

[47] B. Turimov et al., *Dynamical motion of matter around a charged black hole*, *Int. J. Mod. Phys. D* **30** (2021) 2150037 [INSPIRE].

[48] S. Jumaniyozov et al., *Radiative properties and QPOs around charged black hole in Kalb-Ramond gravity*, *Eur. Phys. J. C* **85** (2025) 126 [INSPIRE].

[49] J. Rayimbaev, B. Ahmedov and Z. Stuchlik, *Particles with magnetic dipole moment orbiting magnetized Schwarzschild black holes: Applications to orbits of hot-spots around Sgr A**, *Phys. Dark Univ.* **45** (2024) 101516 [INSPIRE].

[50] S. Jumaniyozov et al., *Black holes surrouTheory of the Relativistic Trajeetories in a Gravitational Field of Schwarzschild nded by PFDM in Kalb-Ramond gravity: from thermodynamics to QPO tests*, *Eur. Phys. J. C* **85** (2025) 797 [INSPIRE].

[51] Y. Hagihara, *Theory of the Relativistic Trajeetories in a Gravitational Field of Schwarzschild*, Jpn. J. Astron. Geophys. **8** (1930) 67.

[52] S. Grunau and V. Kagramanova, *Geodesics of electrically and magnetically charged test particles in the Reissner-Nordström space-time: analytical solutions*, *Phys. Rev. D* **83** (2011) 044009 [arXiv:1011.5399] [INSPIRE].

[53] S. Chandrasekhar, *The Mathematical Theory of Black Holes*, Oxford University Press (1998).

JCAP10(2025)068

[54] H.-P. Nollert, *TOPICAL REVIEW: Quasinormal modes: the characteristic 'sound' of black holes and neutron stars*, *Class. Quant. Grav.* **16** (1999) R159 [INSPIRE].

[55] J. Bicak, Z. Stuchlik and V. Balek, *The motion of charged particles in the field of rotating charged black holes and naked singularities. I*, *Bull. Astron. Inst. Czech.* **40** (1989) 65.

[56] Z. Stuchlik, J. Bicak and V. Balek, *The Shell of Incoherent Charged Matter Falling onto a Charged Rotating Black Hole*, *Gen. Rel. Grav.* **31** (1999) 53.

[57] Z. Stuchlík and A. Kotrlová, *Orbital resonances in discs around braneworld Kerr black holes*, *Gen. Rel. Grav.* **41** (2009) 1305 [arXiv:0812.5066] [INSPIRE].

[58] D. Pugliese, H. Quevedo and R. Ruffini, *Motion of charged test particles in Reissner-Nordström spacetime*, *Phys. Rev. D* **83** (2011) 104052 [arXiv:1103.1807] [INSPIRE].

[59] O. Donmez, *Bondi-Hoyle-Lyttleton accretion around the rotating hairy Horndeski black hole*, *JCAP* **09** (2024) 006 [arXiv:2402.16707] [INSPIRE].

[60] O. Donmez, *Perturbing the Stable Accretion Disk in Kerr and 4D Einstein–Gauss–Bonnet Gravities: Comprehensive Analysis of Instabilities and Dynamics*, *Res. Astron. Astrophys.* **24** (2024) 085001 [arXiv:2310.13847] [INSPIRE].

[61] O. Donmez, F. Dogan and T. Sahin, *Study of Asymptotic Velocity in the Bondi-Hoyle Accretion Flows in the Domain of Kerr and 4-D Einstein-Gauss-Bonnet Gravities*, *Universe* **8** (2022) 458.

[62] O. Donmez, *On the development of the Papaloizou–Pringle instability of the black hole–torus systems and quasi-periodic oscillations*, *Mon. Not. Roy. Astron. Soc.* **438** (2014) 846 [arXiv:1304.0584] [INSPIRE].

[63] F. Koyuncu and O. Dönmez, *Numerical simulation of the disk dynamics around the black hole: Bondi Hoyle accretion*, *Mod. Phys. Lett. A* **29** (2014) 1450115 [INSPIRE].

[64] O. Donmez and F. Dogan, *The Shock Cone Instabilities and Quasi-Periodic Oscillations around the Hartle–Thorne Black Hole*, *Universe* **10** (2024) 152 [INSPIRE].

[65] O. Donmez, *The comparison of alternative spacetimes using the spherical accretion around the black hole*, *Mod. Phys. Lett. A* **39** (2024) 2450076 [arXiv:2405.15467] [INSPIRE].

[66] O. Donmez, *Angular velocity perturbations inducing the Papaloizou-Pringle instability and QPOs in the torus around the black hole*, *Mod. Phys. Lett. A* **32** (2017) 1750108 [arXiv:1703.08175] [INSPIRE].

[67] O. Donmez, *From low- to high-frequency QPOs around the non-rotating hairy Horndeski black hole: Microquasar GRS 1915+105*, *JHEAp* **45** (2025) 1.

[68] O. Donmez and F. Dogan, *Estimating the possible QPOs of M87* from the parameters of a hairy Kerr black hole*, *Phys. Dark Univ.* **46** (2024) 101718 [arXiv:2407.01478] [INSPIRE].

[69] M. Kološ, M. Shahzadi and Z. Stuchlík, *Quasi-periodic oscillations around Kerr-MOG black holes*, *Eur. Phys. J. C* **80** (2020) 133 [INSPIRE].

[70] M. Shahzadi, M. Kološ, Z. Stuchlík and Y. Habib, *Epicyclic oscillations in spinning particle motion around Kerr black hole applied in models fitting the quasi-periodic oscillations observed in microquasars and AGNs*, *Eur. Phys. J. C* **81** (2021) 1067 [arXiv:2104.09640] [INSPIRE].

[71] M. Shahzadi, M. Kološ, R. Saleem and Z. Stuchlík, *Testing alternative spacetimes by high-frequency quasi-periodic oscillations observed in microquasars and active galactic nuclei*, *Class. Quant. Grav.* **41** (2024) 075014 [arXiv:2309.09712] [INSPIRE].

JCAP10(2025)068

[72] G. Mustafa et al., *Testing regular black holes in the framework of asymptotically safe gravity using particle dynamics, QPOs, and shadow constraints*, *Eur. Phys. J. C* **85** (2025) 741 [INSPIRE].

[73] W. Kluzniak and M.A. Abramowicz, *Parametric epicyclic resonance in black hole disks: qpos in micro-quasars*, astro-ph/0203314 [INSPIRE].

[74] O. Straub and E. Sramkova, *Epicyclic oscillations of non-slender fluid tori around Kerr black holes*, *Class. Quant. Grav.* **26** (2009) 055011 [arXiv:0901.1635] [INSPIRE].

[75] C. Bambi, *Probing the space-time geometry around black hole candidates with the resonance models for high-frequency QPOs and comparison with the continuum-fitting method*, *JCAP* **09** (2012) 014 [arXiv:1205.6348] [INSPIRE].

[76] C. Bambi, *Testing the nature of the black hole candidate in GRO J1655-40 with the relativistic precession model*, *Eur. Phys. J. C* **75** (2015) 162 [arXiv:1312.2228] [INSPIRE].

[77] A. Maselli et al., *Testing Gravity with Quasi Periodic Oscillations from accreting Black Holes: the Case of the Einstein-Dilaton-Gauss-Bonnet Theory*, *Astrophys. J.* **801** (2015) 115 [arXiv:1412.3473] [INSPIRE].

[78] K. Jusufi et al., *Quasinormal modes, quasiperiodic oscillations, and the shadow of rotating regular black holes in nonminimally coupled Einstein-Yang-Mills theory*, *Phys. Rev. D* **103** (2021) 024013 [arXiv:2008.08450] [INSPIRE].

[79] M. Ghasemi-Nodehi, M. Azreg-Aïnou, K. Jusufi and M. Jamil, *Shadow, quasinormal modes, and quasiperiodic oscillations of rotating Kaluza-Klein black holes*, *Phys. Rev. D* **102** (2020) 104032 [arXiv:2011.02276] [INSPIRE].

[80] S. Chen, Z. Wang and J. Jing, *Testing gravity of a disformal Kerr black hole in quadratic degenerate higher-order scalar-tensor theories by quasi-periodic oscillations*, *JCAP* **06** (2021) 043 [arXiv:2103.11788] [INSPIRE].

[81] H. Hoshimov et al., *Particle dynamics and quasi-periodic oscillations in the GUP-modified Schwarzschild spacetime: Constraint using micro-quasars data*, *Astropart. Phys.* **165** (2025) 103056 [arXiv:2410.18587] [INSPIRE].

[82] H. Hoshimov et al., *Particle dynamics and quasi-periodic oscillations in the Dyonic ModMax: Constraint using quasars data*, *JHEAp* **45** (2025) 306 [INSPIRE].

[83] E. Ghorani et al., *Constraints on metric-Palatini gravity from QPO data*, *Eur. Phys. J. C* **84** (2024) 1022 [arXiv:2410.04993] [INSPIRE].

[84] X. Lu et al., *Design and Calibration of the High Energy Particle Monitor onboard the Insight-HXMT*, *JHEAp* **26** (2020) 77 [arXiv:1911.01594] [INSPIRE].

[85] W. Yuan et al., *Einstein Probe: Exploring the ever-changing X-ray Universe*, *Sci. Sin. Phys. Mech. Astron.* **48** (2018) 039502.

[86] B.J. Carr, K. Kohri, Y. Sendouda and J. Yokoyama, *New cosmological constraints on primordial black holes*, *Phys. Rev. D* **81** (2010) 104019 [arXiv:0912.5297] [INSPIRE].

[87] M. Sasaki, T. Suyama, T. Tanaka and S. Yokoyama, *Primordial black holes — perspectives in gravitational wave astronomy*, *Class. Quant. Grav.* **35** (2018) 063001 [arXiv:1801.05235] [INSPIRE].

[88] J.C. Niemeyer and K. Jedamzik, *Dynamics of primordial black hole formation*, *Phys. Rev. D* **59** (1999) 124013 [astro-ph/9901292] [INSPIRE].

JCAP10(2025)068

[89] H. Lu, A. Perkins, C.N. Pope and K.S. Stelle, *Black Holes in Higher-Derivative Gravity*, *Phys. Rev. Lett.* **114** (2015) 171601 [arXiv:1502.01028] [INSPIRE].

[90] LIGO Scientific and Virgo collaborations, *Observation of Gravitational Waves from a Binary Black Hole Merger*, *Phys. Rev. Lett.* **116** (2016) 061102 [arXiv:1602.03837] [INSPIRE].

[91] LIGO Scientific and Virgo collaborations, *GW190521: A Binary Black Hole Merger with a Total Mass of* $150M_{\odot}$, *Phys. Rev. Lett.* **125** (2020) 101102 [arXiv:2009.01075] [INSPIRE].

[92] LIGO Scientific and Virgo collaborations, *GW190412: Observation of a Binary-Black-Hole Coalescence with Asymmetric Masses*, *Phys. Rev. D* **102** (2020) 043015 [arXiv:2004.08342] [INSPIRE].

[93] Event Horizon Telescope collaboration, *First M87 Event Horizon Telescope Results. I. The Shadow of the Supermassive Black Hole*, *Astrophys. J. Lett.* **875** (2019) L1 [arXiv:1906.11238] [INSPIRE].

[94] J. Liu et al., *A wide star–black-hole binary system from radial-velocity measurements*, *Nature* **575** (2019) 618 [arXiv:1911.11989] [INSPIRE].

[95] S.W. Hawking, *Black hole explosions?*, *Nature* **248** (1974) 30.

[96] S.W. Hawking, *Particle Creation by Black Holes*, *Commun. Math. Phys.* **43** (1975) 199 [*Erratum ibid.* **46** (1976) 206] [INSPIRE].

[97] S.W. Hawking, *Black holes in general relativity*, *Commun. Math. Phys.* **25** (1972) 152 [INSPIRE].

[98] S.W. Hawking, *Breakdown of Predictability in Gravitational Collapse*, *Phys. Rev. D* **14** (1976) 2460 [INSPIRE].

[99] W.G. Unruh and R. Schutzhold, *On slow light as a black hole analog*, *Phys. Rev. D* **68** (2003) 024008 [gr-qc/0303028] [INSPIRE].

[100] S. Hawking, *Occurrence of singularities in open universes*, *Phys. Rev. Lett.* **15** (1965) 689 [INSPIRE].

[101] G.W. Gibbons and S.W. Hawking, *Classification of Gravitational Instanton Symmetries*, *Commun. Math. Phys.* **66** (1979) 291 [INSPIRE].

[102] S.W. Hawking and G.T. Horowitz, *The Gravitational Hamiltonian, action, entropy and surface terms*, *Class. Quant. Grav.* **13** (1996) 1487 [gr-qc/9501014] [INSPIRE].

[103] M.C. Begelman, R.D. Blandford and M.J. Rees, *Massive black hole binaries in active galactic nuclei*, *Nature* **287** (1980) 307 [INSPIRE].

[104] A. Ori, *Inner structure of a charged black hole: An exact mass-inflation solution*, *Phys. Rev. Lett.* **67** (1991) 789 [INSPIRE].

[105] F. Echeverria, *Gravitational Wave Measurements of the Mass and Angular Momentum of a Black Hole*, *Phys. Rev. D* **40** (1989) 3194 [INSPIRE].

[106] S.W. Hawking, *Black Holes From Cosmic Strings*, *Phys. Lett. B* **231** (1989) 237 [INSPIRE].

[107] A. Strominger, *Black hole statistics*, *Phys. Rev. Lett.* **71** (1993) 3397 [hep-th/9307059] [INSPIRE].

[108] W.K.H. Panofsky, *Needs versus means in high-energy physics*, *Phys. Today* **33** (1980) 24 [INSPIRE].

[109] P. Hajicek, *On the Origin of Hawking Radiation*, *Phys. Rev. D* **36** (1987) 1065 [INSPIRE].

JCAP10(2025)068

[110] N. Popławski, *Universe in a Black Hole in Einstein-Cartan Gravity*, *Astrophys. J.* **832** (2016) 96 [arXiv:1410.3881] [INSPIRE].

[111] D.V. Fursaev, *Temperature and Entropy of a Quantum Black Hole and Conformal Anomaly*, *Phys. Rev. D* **51** (1995) 5352 [INSPIRE].

[112] R. Konoplya and A. Zhidenko, *Detection of gravitational waves from black holes: Is there a window for alternative theories?*, *Phys. Lett. B* **756** (2016) 350 [arXiv:1602.04738] [INSPIRE].

[113] S.W. Hawking, *The Quantum State of the Universe*, *Nucl. Phys. B* **239** (1984) 257 [INSPIRE].

[114] S.W. Hawking, *Black Holes and Thermodynamics*, *Phys. Rev. D* **13** (1976) 191 [INSPIRE].

[115] S.W. Hawking and D.N. Page, *Thermodynamics of Black Holes in anti-De Sitter Space*, *Commun. Math. Phys.* **87** (1983) 577 [INSPIRE].

[116] P.C.W. Davies, *Thermodynamics of black holes*, *Rept. Prog. Phys.* **41** (1978) 1313 [INSPIRE].

[117] J.D. Bekenstein, *Statistical Black Hole Thermodynamics*, *Phys. Rev. D* **12** (1975) 3077 [INSPIRE].

[118] S.W. Hawking, *Black holes in the Brans-Dicke theory of gravitation*, *Commun. Math. Phys.* **25** (1972) 167 [INSPIRE].

[119] D.L. Wiltshire, *Black Holes in String Generated Gravity Models*, *Phys. Rev. D* **38** (1988) 2445 [INSPIRE].

[120] A. Ashraf et al., *Quasi-periodic oscillations and particle motion around charged black hole surrounded by a cloud of strings and quintessence field in Rastall gravity*, *Phys. Scripta* **99** (2024) 065011 [INSPIRE].

[121] D. Iosifidis and F.W. Hehl, *Motion of test particles in spacetimes with torsion and nonmetricity*, *Phys. Lett. B* **850** (2024) 138498 [arXiv:2310.15595] [INSPIRE].

[122] G. Mustafa et al., *Observational signature of QPOs with particle motion around non-commutative Schwarzschild black hole surrounded by perfect fluid dark matter*, *Phys. Dark Univ.* **46** (2024) 101644 [INSPIRE].

[123] G. Mustafa et al., *Orbital motion, epicyclic oscillations, and collision of particles around conformally coupled charged black hole*, *Phys. Dark Univ.* **46** (2024) 101647 [INSPIRE].

[124] G. Mustafa and S.K. Maurya, *Testing strong gravitational lensing effects of various supermassive compact objects for the static and spherically symmetric hairy black hole by gravitational decoupling*, *Eur. Phys. J. C* **84** (2024) 686 [INSPIRE].

[125] D.-K. Lian et al., *Strong decays of $T^a_{c\bar{s}0}(2900)^{++/0}$ as a fully open-flavor tetraquark state*, *Eur. Phys. J. C* **84** (2024) 1 [arXiv:2302.01167] [INSPIRE].

[126] I. Kraljevski et al., *How to Do Machine Learning with Small Data? — A Review from an Industrial Perspective*, arXiv:2311.07126.

[127] L. Iorio and M.L. Ruggiero, *Phenomenological constraints on the Kehagias-Sfetsos solution in the Horava-Lifshitz gravity from solar system orbital motions*, *Int. J. Mod. Phys. A* **25** (2010) 5399 [arXiv:0909.2562] [INSPIRE].

[128] F.S.N. Lobo, T. Harko and Z. Kovács, *Solar System Tests of Hořava-Lifshitz Black Holes*, arXiv:1001.3517 [INSPIRE].

[129] G.J. Olmo, *Palatini Approach to Modified Gravity: f(R) Theories and Beyond*, *Int. J. Mod. Phys. D* **20** (2011) 413 [arXiv:1101.3864] [INSPIRE].

JCAP10(2025)068

[130] LIGO Scientific and Virgo collaborations, *Observation of Gravitational Waves from a Binary Black Hole Merger*, *Phys. Rev. Lett.* **116** (2016) 061102 [arXiv:1602.03837] [INSPIRE].

[131] Event Horizon Telescope collaboration, *First M87 Event Horizon Telescope Results. IV. Imaging the Central Supermassive Black Hole*, *Astrophys. J. Lett.* **875** (2019) L4 [arXiv:1906.11241] [INSPIRE].

[132] C. Bambi, *Black Holes: A Laboratory for Testing Strong Gravity*, Springer (2017) [DOI:10.1007/978-981-10-4524-0].

[133] M. Zhou et al., *Testing conformal gravity with the supermassive black hole in 1H0707-495*, *Phys. Rev. D* **98** (2018) 024007 [arXiv:1803.07849] [INSPIRE].

[134] A. Tripathi et al., *Constraints on the Spacetime Metric around Seven "Bare" AGNs Using X-Ray Reflection Spectroscopy*, *Astrophys. J.* **874** (2019) 135 [arXiv:1901.03064] [INSPIRE].

[135] J.F. Steiner et al., *The Spin of the Black Hole Microquasar XTE J1550-564 via the Continuum-Fitting and Fe-Line Methods*, *Mon. Not. Roy. Astron. Soc.* **416** (2011) 941 [arXiv:1010.1013] [INSPIRE].

[136] J.F. Steiner et al., *The Constant Inner-Disk Radius of LMC X-3: A Basis for Measuring Black Hole Spin*, *Astrophys. J. Lett.* **718** (2010) L117 [arXiv:1006.5729] [INSPIRE].

[137] L. Gou et al., *Confirmation Via the Continuum-Fitting Method that the Spin of the Black Hole in Cygnus X-1 is Extreme*, *Astrophys. J.* **790** (2014) 29 [arXiv:1308.4760] [INSPIRE].

[138] X. Zhang and Q.G. Gao, *The fundamental plane of FSRQs based on the black hole spin-mass energy*, *Astrophys. Space Sci.* **368** (2023) 69.

[139] S. Chen, M. Wang and J. Jing, *Chaotic motion of particles in the accelerating and rotating black holes spacetime*, *JHEP* **09** (2016) 082 [arXiv:1604.02785] [INSPIRE].

[140] K. Hashimoto and N. Tanahashi, *Universality in Chaos of Particle Motion near Black Hole Horizon*, *Phys. Rev. D* **95** (2017) 024007 [arXiv:1610.06070] [INSPIRE].

[141] S. Dalui, B.R. Majhi and P. Mishra, *Presence of horizon makes particle motion chaotic*, *Phys. Lett. B* **788** (2019) 486 [arXiv:1803.06527] [INSPIRE].

[142] Z. Stuchlík et al., *Influence of Cosmic Repulsion and Magnetic Fields on Accretion Disks Rotating around Kerr Black Holes*, *Universe* **6** (2020) 26.

[143] D. Pugliese, H. Quevedo and R. Ruffini, *Motion of charged test particles in Reissner-Nordström spacetime*, *Phys. Rev. D* **83** (2011) 104052 [arXiv:1103.1807] [INSPIRE].

[144] A. Jawad, F. Ali, M. Jamil and U. Debnath, *Dynamics of Particles Around a Regular Black Hole with Nonlinear Electrodynamics*, *Commun. Theor. Phys.* **66** (2016) 509 [arXiv:1610.07411] [INSPIRE].

[145] S. Hussain and M. Jamil, *Timelike geodesics of a modified gravity black hole immersed in an axially symmetric magnetic field*, *Phys. Rev. D* **92** (2015) 043008 [arXiv:1508.02123] [INSPIRE].

[146] G.Z. Babar, M. Jamil and Y.-K. Lim, *Dynamics of a charged particle around a weakly magnetized naked singularity*, *Int. J. Mod. Phys. D* **25** (2015) 1650024 [arXiv:1504.00072] [INSPIRE].

[147] M. Bañados, J. Silk and S.M. West, *Kerr Black Holes as Particle Accelerators to Arbitrarily High Energy*, *Phys. Rev. Lett.* **103** (2009) 111102 [arXiv:0909.0169] [INSPIRE].

[148] M. De Laurentis et al., *Test-particle dynamics in general spherically symmetric black hole spacetimes*, *Phys. Rev. D* **97** (2018) 104024 [arXiv:1712.00265] [INSPIRE].

JCAP10(2025)068

[149] B. Turimov, B. Ahmedov, M. Kološ and Z. Stuchlík, *Axially symmetric and static solutions of Einstein equations with self-gravitating scalar field*, *Phys. Rev. D* **98** (2018) 084039 [arXiv:1810.01460] [INSPIRE].

[150] A. Ditta et al., *Testing metric-affine gravity using particle dynamics and photon motion*, *Phys. Dark Univ.* **41** (2023) 101248 [arXiv:2303.05438] [INSPIRE].

[151] A. Ditta, T. Xia and M. Yasir, *Particle motion and lensing with plasma of acoustic Schwarzschild black hole*, *Int. J. Mod. Phys. A* **38** (2023) 2350041 [INSPIRE].

[152] A. Ditta et al., *Particle dynamics and fundamental frequencies of black hole coupled with a nonlinear electrodynamics field*, *JHEAp* **43** (2024) 51 [INSPIRE].

[153] A. Ditta et al., *Particle dynamics and weak gravitational lensing around nonlinear electrodynamics black hole*, *Chin. J. Phys.* **83** (2023) 664 [INSPIRE].

[154] A. Ditta et al., *Particle dynamics, black hole shadow and weak gravitational lensing in the f (Q) theory of gravity*, *Commun. Theor. Phys.* **75** (2023) 125404 [INSPIRE].

[155] A. Alonso-Bardaji, D. Brizuela and R. Vera, *Nonsingular spherically symmetric black-hole model with holonomy corrections*, *Phys. Rev. D* **106** (2022) 024035 [arXiv:2205.02098] [INSPIRE].

[156] Z.S. Moreira, H.C.D. Lima Junior, L.C.B. Crispino and C.A.R. Herdeiro, *Quasinormal modes of a holonomy corrected Schwarzschild black hole*, *Phys. Rev. D* **107** (2023) 104016 [arXiv:2302.14722] [INSPIRE].

[157] A. Ashraf et al., *Imprints of quantum gravity on periastron precession and trajectories around a black hole*, *Phys. Dark Univ.* **47** (2025) 101787 [INSPIRE].

[158] G. Mustafa et al., *Orbital motion and epicyclic oscillations around a black hole with magnetic charge*, *Phys. Dark Univ.* **47** (2025) 101765 [INSPIRE].

[159] G. Mustafa et al., *Epicyclic oscillations around slowly rotating charged black hole in Bumblebee gravity*, *Phys. Dark Univ.* **47** (2025) 101753 [INSPIRE].

[160] C.W. Misner, K.S. Thorne and J.A. Wheeler, *Gravitation*, W.H. Freeman (1973).

[161] S. Chandrasekhar, *The Mathematical Theory of Black Holes*, Oxford University Press (1983).

[162] D.C. Wilkins, *Bound Geodesics in the Kerr Metric*, *Phys. Rev. D* **5** (1972) 814 [INSPIRE].

[163] W. Tichy and P. Marronetti, *A Simple method to set up low eccentricity initial data for moving puncture simulations*, *Phys. Rev. D* **83** (2011) 024012 [arXiv:1010.2936] [INSPIRE].

[164] S. Kato, J. Fukue and S. Mineshige, *Black-Hole Accretion Disks: Towards a New Paradigm*, *Publications of the Astronomical Society of Japan*, Kyoto University Press (1990), https://www.kyoto-up.or.jp/books/9784876987405.html?lang=en.

[165] F.D. Ryan, *Gravitational waves from the inspiral of a compact object into a massive, axisymmetric body with arbitrary multipole moments*, *Phys. Rev. D* **52** (1995) 5707 [INSPIRE].

[166] J. Levin and G. Perez-Giz, *Homoclinic Orbits around Spinning Black Holes. I. Exact Solution for the Kerr Separatrix*, *Phys. Rev. D* **79** (2009) 124013 [arXiv:0811.3814] [INSPIRE].

[167] M.A. Abramowicz and P.C. Fragile, *Foundations of Black Hole Accretion Disk Theory*, *Living Rev. Rel.* **16** (2013) 1 [arXiv:1104.5499] [INSPIRE].

[168] O. Donmez, *Evolution of Shock Structures and QPOs After Halting BHL Accretion onto Kerr Black Hole*, arXiv:2503.16665 [INSPIRE].

[169] T.E. Strohmayer, *Discovery of a second high frequency qpo from the microquasar grs 1915+105*, *Astrophys. J. Lett.* **554** (2001) L169 [astro-ph/0105338] [INSPIRE].

JCAP10(2025)068

[170] H. Liu et al., *Testing evolution of LFQPOs with mass accretion rate in GRS 1915+105 with Insight-HXMT*, *Astrophys. J.* **909** (2021) 63 [arXiv:2012.01825] [INSPIRE].

[171] S. Majumder et al., *Wide-band view of high-frequency quasi-periodic oscillations of GRS 1915+105 in 'softer' variability classes observed with AstroSat*, *Mon. Not. Roy. Astron. Soc.* **512** (2022) 2508 [arXiv:2203.02710] [INSPIRE].

[172] S.E. Motta and T.M. Belloni, *Rethinking the 67 Hz QPO in GRS 1915+105: Type C quasi-periodic oscillations at the innermost stable circular orbit*, *Astron. Astrophys.* **684** (2024) A209 [arXiv:2307.00867] [INSPIRE].

[173] R.A. Remillard et al., *RXTE Observations of 0.1–300 HZ Quasi-periodic Oscillationsin the Microquasar GRO J1655-40*, *Astrophys. J.* **522** (1999) 397.

[174] S.E. Motta et al., *Precise mass and spin measurements for a stellar-mass black hole through X-ray timing: the case of GRO J1655-40*, *Mon. Not. Roy. Astron. Soc.* **437** (2014) 2554 [arXiv:1309.3652] [INSPIRE].

[175] P. Varniere and J. Rodriguez, *Looking for the Elusive 3:2 Ratio of High-frequency Quasi-periodic Oscillations in the Microquasar XTE J1550-564*, *Astrophys. J.* **865** (2018) 113 [arXiv:1808.06823] [INSPIRE].

[176] D. Altamirano and T. Strohmayer, *Low Frequency (11 mHz) Oscillations in H1743-322: A New Class of Black Hole QPOs?*, *Astrophys. J. Lett.* **754** (2012) L23 [arXiv:1206.0476] [INSPIRE].

JCAP10(2025)068